The Creation and Simulation of a Risley Prism Assembly

Ву

Kevin Tyler Galvan, B.S. EE

A Thesis

In

Electrical Engineering

Submitted to the Graduate Faculty
Of Texas Tech University in
Partial Fulfillment of
The Requirements for
The Degree of
Master of Science in Electrical Engineering

@ 2019, Kevin T. Galvan

ACKNOWLEDGEMENTS

For my acknowledgements I would like to mention the engineers and management at NASA Goddard Spaceflight Center. In particular, the electro-mechanical systems branch, code 544. During my time working at this center, these people have helped influence the design, and creation of the following project. In specific I would like to thank Umesh Patel, the branch manager of code 544, for bringing me into the branch and offering school and career advice throughout my internships. Additionally, Rajeev Sharma, the project lead for the following design, who managed the project and provided ideas for the assembly. Lastly, for the project, I am grateful for the work done by Sam Zhao, who helped in the creation and simulation of the design. Finally, I would like to thank my master thesis committee for taking the time to review the project and thesis paper. Also, for offering advice and providing guidance through the thesis process.

Table of Contents

ACKN	NOWLEDGEMENTS	iii
Abstra	act	vi
List of	of Figures	vii
I. I	INTRODUCTION	1
II. P	PROJECT BACKGROUND	3
III.	PROJECT OVERVIEW	5
A.	Risley Prism	6
В.	Control System	8
C.	Requirnments and Procedure	10
IV.	DESIGN	12
A.	Motor	12
B.	Drives and Controllers	17
C.	Encoder	20
V. (CONTROL	21
A.	Velocity Loop	21
В.	Coding	24
VI.	SCANNER SIMULATION	28
A.	Overview	28
В.	Motor Drivers	29
C	Motor	33

D.	Encoder System	36
E.	Phase Equation	37
F.	Simulation Script	38
G.	Simulation Graphs	39
VII.	RESULTS	42
A.	Performance	43
B.	Simulation Comparison	49
VIII.	CONCULSION AND FUTURE WORK	55
IX.	REFERENCES	58

ABSTRACT

Intentions of humans revisiting the moon, exploring new planets, and the ever sought out goal of landing humans on Mars is a focus for NASA. With the most recent human missions being the Apollo missions in the 1960's-1970's, upgrades to previous landers are a continuing project. One of the most important and difficult parts of these missions is the landing. An unknown environment and terrain provide challenges for the crew or lander, that may result in broken instruments, overuse of fuel and worst of all, loss of life. The following paper highlights the work done to build a demo lidar scanner for landers and other spacecrafts that touchdown on an alien surface. This instrument intends to provide key information about the surface by creating a three-dimensional map of the terrain in a couple of seconds. Information that can then be used as feedback to the guidance computer and pilots to make an informed decision about a safe landing site. The work is being undertaking by a team at Goddard Spaceflight Center under the electromechanical systems branch, and the following represents the work done to create a prototype scanner.

LIST OF FIGURES

Figure 1: Apollo Lander Control System [1]	1
Figure 2: InSight Landing Protocol [2]	2
Figure 3: Hazard Detection Example [3]	4
Figure 4: Risley Prism Operation [4]	6
Figure 5: Risely Prism Patterns [4]	7
Figure 6: General System Block Diagram	8
Figure 7: Torque Velocity Example [7]	14
Figure 8: Mounted Demo Motor	16
Figure 9: Controller and Driver System	19
Figure 10: General Control Block Diagram	22
Figure 11: Control Panel	24
Figure 12: Software General Block Diagram	25
Figure 13: MATLAB RPA Simulation	28
Figure 14: Simulation Motor Driver 1	29
Figure 15: Simulation Motor Driver 2	31
Figure 16: Simulation Motor Model	33
Figure 17: Simulated Scan Pattern	38
Figure 18: Motor Simulated Scanning Velocities	40
Figure 19: Motor Simulated Velocity Profiles	40
Figure 20: Simulated Phase Voltages	41
Figure 21: Simulated Phase Error Profiles	41
Figure 22: Full System Setup	42

Figure 23: Velocity Error Vs. Velocity	43
Figure 24: Power Vs. Speed	45
Figure 25: Long Exposer Scan Pattern	47
Figure 26: Reality Vs. Simulation Power	50
Figure 27: Measured Winding Current and Generated Torque	52
Figure 28: Power After Correction	53
Figure 29: Voltage After Correction	54
Figure 30: Winding Current After Correction	54
Figure 31: Torque After Correction	55

I. INTRODUCTION

The Surveyor program, sponsored by NASA, were the first robotic spacecrafts to perform a soft landing on an alien surface. Through the years of 1966-1968, a series of seven landers were sent to the Moon with the purpose of scouting the way for the Apollo missions, testing new equipment, and a new landing method. Each were sent to land on a different part of the Moon which had been scouted out beforehand. Out of the seven, two of the landers were unsuccessful, one lost radio communication after landing and the other crashed during a midcourse correction in the landing maneuver. The other successful landers determined safe landing locations, tested the soil, and proved the landing capabilities and methods needed for the Apollo missions. These landers lead to the success of the Apollo program carried out from 1967-1972. With the goal of landing the first thumans on the Moon. The Apollo landers used the same radar based landing technique, that the surveyor program used, in tangent with a guidance system and other instruments, as seen in Figure 1.

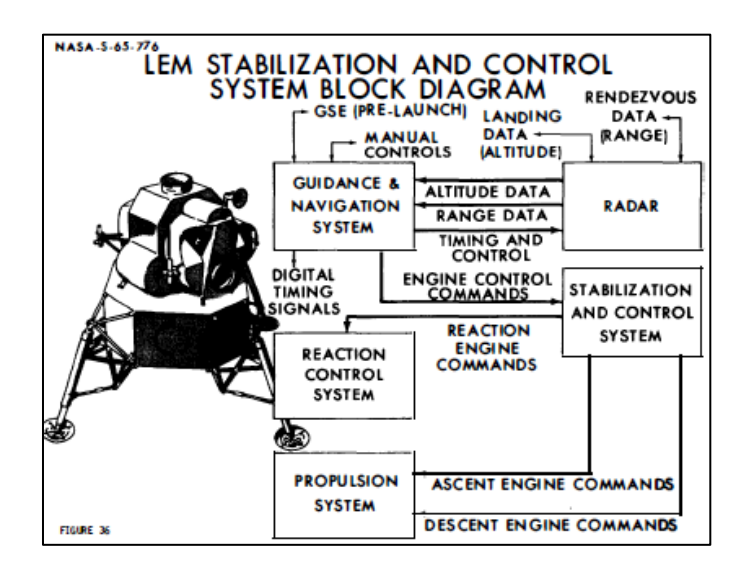


Figure 1: Apollo Lander Control System [1]

The landing radar (LR) along with an inertial measurement unit (IMU) are the main sensors in the landing system that communicate with the guidance computer. The LR is a four beam continuous wave (CW) doppler radar with three components measuring velocities in the X, Y, and Z axis, and the other beam measuring altitude. The guidance system is updated by the LR once the altitude reaches 25,000 ft and a velocity of 15,000 ft. Based on the feedback from the LR and IMU the guidance computer controls the reaction control system (RCS), ascent engine, and descent engine to steer the lander. RCS is a series of thrusters that allow the lander to move directions roll, pitch, and yaw. Altitude and velocity control are maintained through the main thrusters. Final touch down is detected from hanging probes that are attached to the lander's feet. Once the ground is detected from the probes the thruster is shut off and the landing is complete [1].

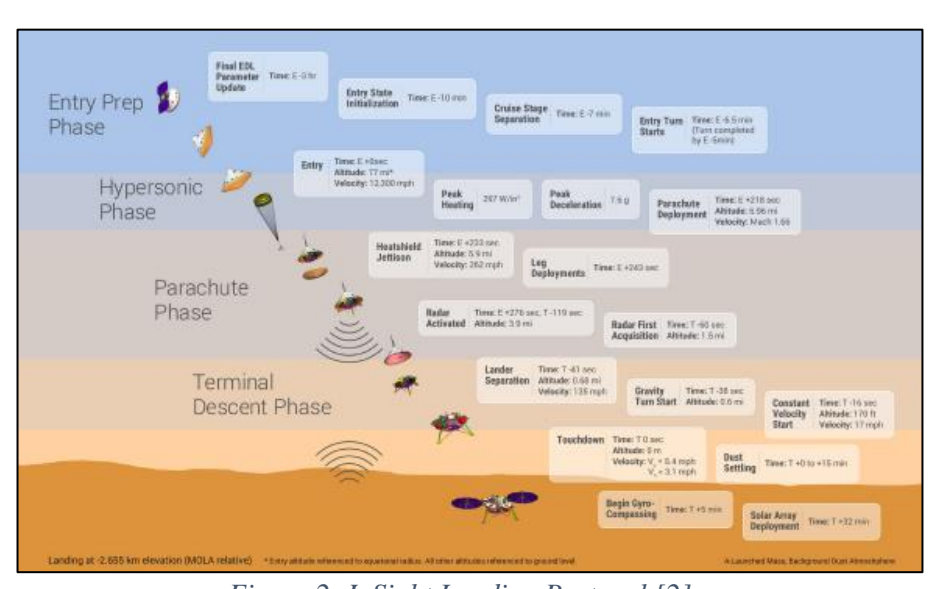


Figure 2: InSight Landing Protocol [2]

NASA continues to use a radar based landing system with new spacecrafts being sent today. Updates and performance capabilities have been added since the time of the Apollo missions, but the concept remains the same. The most recent lander, InSight, launched to Mars on May 5, 2018, utilizes the addition of a parachute and ejectable heatshield during

the decent phase. This reduces the need for thruster fuel, final landing weight, and allows for an easier controlled landing. After two minutes from the parachute deployment and one minute before landing, a radar is activated and begins sensing altitude and velocity. The guidance computer then fires 12 descent engines and provides commands to reduce horizontal and vertical velocities. With this system, InSight completed the landing on November 26, 2018 [2].

Radar landing based approach has been successful in most of the missions, but the full system is lacking in hazard detection capabilities. Undetected objects such as craters, rock formations, and other geological structures have the potential to damage the landers instruments or thrusters upon touchdown. The loss of which damages the mission and potentially leads to loss of life during a manned mission. These difficulties come when the surface of the terrestrial object is unknown, and a landing zone cannot be scouted before launch. For example, the Apollo missions used the Surveyor program and InSight used a satellite named TESS, Transitioning Exoplanet Survey Satellite, to find a safe landing zone [2]. A planet without a satellite observing the location or pre-scouting mission makes determining landing zones difficult. Additional, deep space exploration has the same issue if the planet is too far to view in detail, a radar landing system alone may have issues on touchdown. Therefore, there is a need for a system capable of detecting these hazards to allow for safer spacecraft landings and giving the potential to land in more difficult areas.

II. PROJECT BACKGROUND

The need for technological advancement in the areas of high precision landing, is a topic NASA has made steps towards. A project team named (SPLICE), Safe and Precise Landing Integrated Capabilities Evolution, seeks to advance, and infuse precision lading,

and hazard avoidance into spaceflight missions. Efforts include improving sensors, guidance simulation tools, control system performance, computing capabilities, and more. The team currently is working on a couple projects, a navigation Doppler lidar (NDL), hazard detection lidar (HDL), and descent and landing computer (DLC) [3].

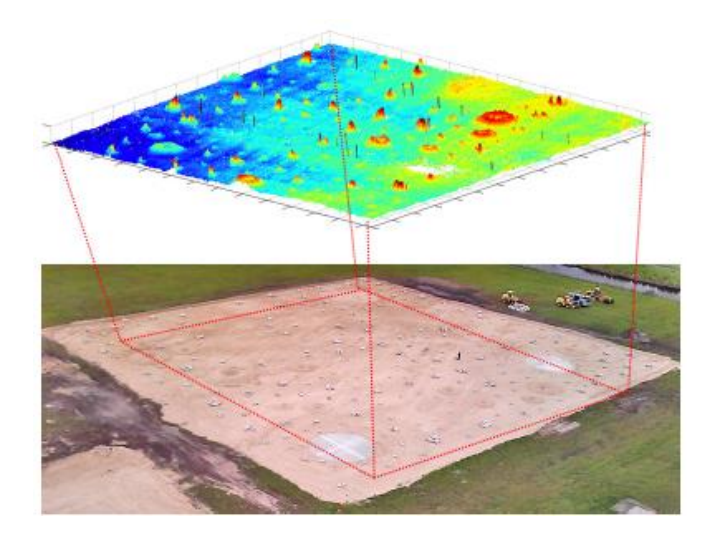


Figure 3: Hazard Detection Example [3]

The HDL project plans to be capable of generating a real-time, three-dimensional map of the terrain within a few seconds, from a range of at least 500 meters. An example of a generated map is shown in Figure 3 above. For the scanner, resolution accuracy intends to be able to identify hazards that have the potential of damaging the lander. This project is in competition phase where different NASA campuses and contractors submit proposals to win funding for the projects. These projects start out as Internal Research and Development (IRAD) projects then work the way up to spaceflight project once the prototype meets requirements.

Currently, a team at Goddard Spaceflight Center is undergoing the work to build a demo version of the HDL project. The electro-mechanical systems branch, code 544, at Goddard has heritage when it comes to lidar scanners. From the missions GEDI, Global

Ecosystem Dynamics Investigation Lidar, and GLAS, Geoscience Laser Altimeter System. GEDI of which has the highest resolution and densest sampling of any lidar in orbit. Used to 3D image remote forests around the globe in order to understand how ecosystems store and release carbon.

For the project the team divided the work into three groups; sensor design and performance analysis, system engineering, and discipline lead engineers. Sensor team focuses on the architectural design and simulations for the sensor. Systems engineering handle the higher level elements such as system integration, radiation concerns, and planetary protection. Discipline leads work on building sections of the lidar scanner such as, mechanical structures, laser, optical components, fiber optics, and a Risley prism assembly. The following explains the work done by the Risley prism assembly (RPA) team.

III. PROJECT OVERVIEW

Lidar, light detection and ranging, is a method used for surveying an area. A pulsed laser illuminates the target from a distance used to measure an objects range. The reflected light is collected by a detector and the difference in return times and wavelengths give information on the targets distance. For area mapping a series of these pulses are put together in order to form a 3D map of the area. To completely scan a target, the precise control of the lasers position is critical. Typically, in an optical system, moving mirrors, prisms, lenses, or diffractive gratings are used to control the lasers final position. This process is known as beam steering and the chosen method by the optical team is utilizing Risley prisms. The RPA team oversees the construction of the pointing mechanism for the lidar scanner.

A. Risley Prism

The concept of Risley prisms involves the use of two wedged prisms that steer the laser. Each prism has a refracting angle that bends the light upon exiting. Although this is not a new idea, the process has become popular for fast response, fast scan speeds, clear aperture, wide field of view and lower power operations [4]. These benefits are important for a scanner that is required to finishes within a few seconds and scan a large area. Also, using this method, for the implementation on a spacecraft requires the use of low power to conserve energy.

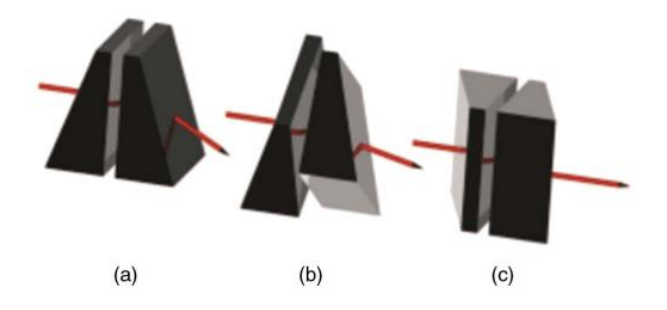


Figure 4: Risley Prism Operation [4]

Operation and general technique of the prisms is shown in the figure above. The relative phasing of the first prism to the second prism controls the final angle that the laser beam exits. In Figure 4 (a) the maximum angle is shown when the prisms are aligned with no phase difference. Output angle in this position is equal to twice the refracted angle of a single prism. Once the phasing starts to deviate the bending of the laser becomes less and less, based off the rotational angle. Figure 4 (c) shows the other minimal diffraction angle once the pair becomes out of phase by 180°. The first and the last case give the range angle for the scanner.

$$y(\theta_1, \theta_2) = r_1 * \sin(\theta_1) + r_2 * \sin(\theta_2)$$

$$x(\theta_1, \theta_2) = r_1 * \cos(\theta_1) + r_2 * \cos(\theta_2)$$

$$(1)$$

With the relationship between the two prisms known, the components form a conceptual cone of possibilities that start at the output of the last prism. The X and Y positions are defined through the equation shown above (1) [5]. Where r_1 and r_2 define the output radius from each prism and θ_1 and θ_2 are the angled positions of the prisms. In the time domain, $\theta = \omega t$, therefore the equation can be written in terms of angular velocity and time as shown in the equation below (2).

$$y(\omega_1, \omega_2) = r_1 * \sin(\omega_1 t) + r_2 * \sin(\omega_2 t)$$

$$x(\omega_1, \omega_2) = r_1 * \cos(\omega_1 t) + r_2 * \cos(\omega_2 t)$$
(2)

Utilizing the relationship in terms of velocity creates a time dependent equation for the prisms. Based on the equations there is a predictable relationship between the output position of the laser and speed of rotation of the prisms. When mapped with velocities the output creates repeatable patterns depending on the velocity relationship of the prisms. The images below show possible patterns that are created utilizing the equations in (2). Figure 5 (a) shows $\frac{\omega_1}{\omega_2} = -2$ a Trifolium is created, (b) when $\frac{\omega_1}{\omega_2} = \sqrt{2}$ Rose Curves are made, (c) shows when $\frac{\omega_1}{\omega_2} = 2$ a Limaçon shape is formed.

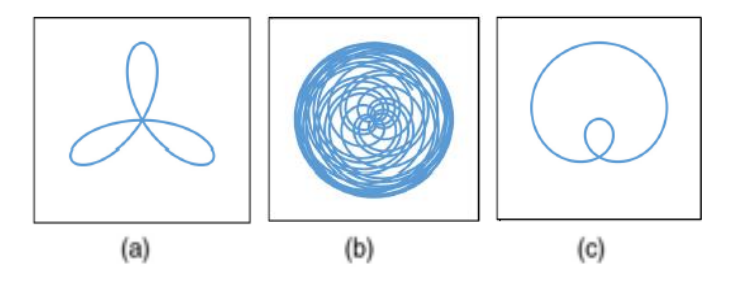


Figure 5: Risely Prism Patterns [4]

In order to determine the best pattern for area coverage, MATLAB scripts were created to compare candidates. Utilizing a discontinues beam creates patterns made from points

instead of a continuous line. The pattern with the best area coverage then is found through the calculations of spots per pixel. A quadratic relationship, based on a predetermine equation, between the first and second prism is found to have the most area coverage for the project. An example of the equation (3) is shown below where θ_d is the phase difference, θ_1 and θ_2 are the phases of each prism, t is time, and the other variables are constants.

$$\theta_d = \theta_1 - \theta_2 = at^3 + bt^2 + ct + d \tag{3}$$

B. Control System

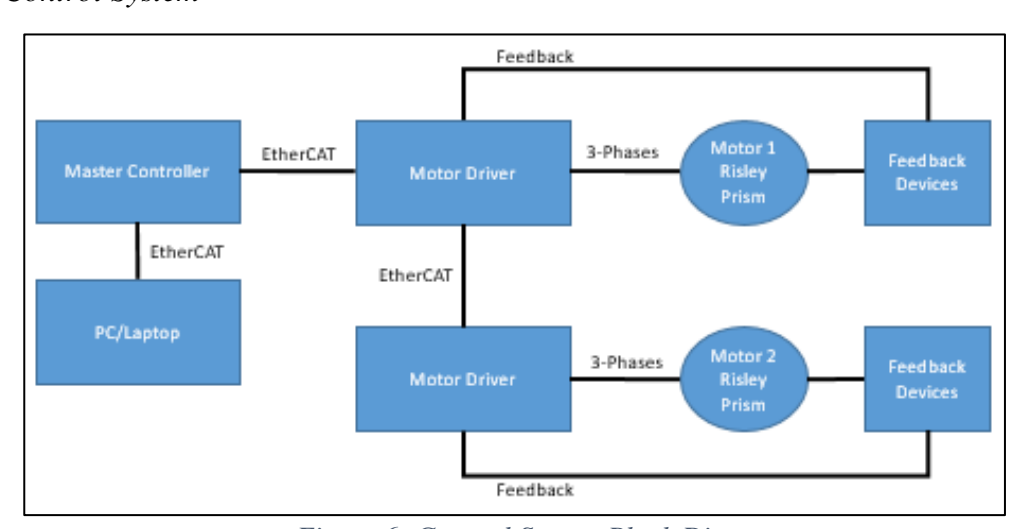


Figure 6: General System Block Diagram

To create the scan patterns the prims are controlled through velocity and phasing. For this, an optical mechanical design is created to house the Risley prisms. The figure above shows the general block diagram of the system. Each prism is housed inside a motor to control phase and velocity. Utilizing feedback devices, the relative phase or velocity of one prism to the other is known and controlled through a series of devices. The entire system utilizes a laptop or PC in order to control the prims. Overall it acts as the interface between the user and the hardware. Providing a GUI for the motor controller and drives from an installed software. The coding is written in free form ladder diagram, special to

the system, and has an interface like LabView. Through an internet connection the PC interfaces the master controller. Since the drives and controller have a unique IP address. This is done either through a standard EtherCAT wired connection or remote access over Wi-Fi.

The master controller acts as the brains of the operation and interfaces the drives. The drives send back important information from the motors such as, velocity, winding current, voltage, position, and other motor parameters. This gets interpreted by the controller providing the information back to the user through the software. If the controller receives a parameter that does not follow or match the codes instructions, error flags are displayed. This is also the case if there is a fault on the drives such as over current, low bus power, short circuiting, and other errors.

Through an EtherCAT wired connection the motor drives send and receive commands and readings to and from the motors. The EtherCAT connection is daisy chained together and all the information passes through one line. These drivers handle the actual control of the motors, while the master controller only sends set point parameters. Additional information on operation of the motor drivers and master control is further explained in the design section.

The last part of the control system is the feedback devices. These parts are directly connected to each motor driver and are used in the control loops to maintain velocity or position. The main feedback from the motors is the hall effect sensors. Start position and commutation are derived from these three magnetic sensors, which are positioned on the stator to detect rotor position. Through heavy interpolation these sensors can be used for velocity feedback during higher motor speeds. Limitations occur at lower velocities due

to the low resolution of feedback from three hall sensors. An encoder provides more accurate information than the hall effect sensors and is needed for position control of the prisms. A thermistor inside the motor provides thermal information. Although the run time of the motor is short with a limited scanning time, the data gives an idea if there is a fault or issue in the system. Since motor overheating is a rare case with a short run time.

C. Requirnments and Procedure

The design had a series of tasks it needed to perform, split into three phases of the scanning process. Phase one, both motors come up to a desired speed and maintain a tight velocity lock. Phase two, the first motor maintains the same velocity while the second motor becomes out of phase by a certain amount relative to the first motor. Phase three, the second motor preforms a phase difference move based on the ideal scan pattern for area coverage. The first motor maintains the same phase and velocity while the second motor slows and follows a phase difference equation. These are the steps the RPA needed to run to perform the scan.

The requirements for the procedure listed above focuses on the precision of the scan pattern and power consumption. For the first phase, the settling time for the motors to reach their desired speeds is critical. The longer the motors take, the earlier they need to be turned on during the decent phase. This consumes power over time from the high speeds the motors need to reach for the scan. Although with a shorter settling times and higher acceleration the more instantaneous power is needed. Therefore, there is a tradeoff between the startup time and power consumption. This subject is being investigated through simulation and demo builds to determine the best settling time versus power. During this phase, the lock on the settling speed is also important. Variability in the top

speed causes errors in the phase difference between the prisms. An unsteady velocity control causes wobble in the output of the lasers ideal position leading to missed points and or uneven coverage on the surface.

For the second phase, when the second motor locks to an out of phase position to motor one, the requirements are like the first phase. Again, the lock in velocity is critical to reduce phase errors. This time the position is also a variable to consider. The lock to an initial phase difference is to start the scanner at the widest possible point. If there was a $100 \, m^2$ box, the laser would start at the edges of the box and work its way inwards. Since the patterns are a function of time, starting at the wrong initial phase difference would start the scan in the wrong area of the terrain. Although the scans are repeatable and overtime the position would be filled, there is also a time consideration. Since the scanner is limited to a couple of seconds, a misalignment in the starting phase difference causes the scan pattern to miss an area within the terrain.

The final phase is the most important for the science portion of the project. In order to accurately scan the area, the phasing of the second motor needs to have as little error as possible compared to the desired equation. In addition, the velocity also needs little error since it relates directly to the phase difference equation through a derivative. For this portion the second motor slows to perform the phase difference. This is chosen versus speeding up the motor due to power, torque, and control purposes. Allowing the control to do less to maintain the tight phasing requirements.

Lastly, after the completion of the science phase the shutdown of the motors is considered. During this time the motors are still consuming power until coming to a complete stop. There are a couple options for this process. The motors can be shut off

through a hard breaking function where reverse voltage is applied to the motor for an immediate stop. This involves the use of extra power but is the fastest way to stop motion. Another option is reducing the power overtime and decelerating the motors. This option offers the most control over the shutdown time but again uses power to turn off the motors. The last option is turning off the power completely and letting the motors free spin down to zero velocity. This uses the least amount of power but also the least amount of control on turn off. These options are being considered and more research is needed to decide on the best process.

IV. DESIGN

When designing IRAD projects the first step is to find commercial of the shelf (COTS) parts that can perform the needed tasks. This allows for a rapid prototype of the RPA to be created in a shorter amount of time. Rather than waiting for the design and testing of driver and controller cards along with specialized motors and encoders. Using the COTS parts also helps give insight into the control of the motors, the motor performance, power requirements, and other aspects of the project. The control system requires a couple main components two motors, two encoders, two motor drivers, and a controller.

A. Motor

For the motor there are a couple of different types for consideration, stepper, brushed and brushless motors. A stepper motor provides precise and discrete steps depending on the number of poles within the motor. Used for applications such as 3D printers, milling machines, robotics, and more. Electrical pulses from a driver provide commutation for each step in a specific sequence to drive the motor. Although precise positioning is need for the prisms these motors typically operate at lower speeds and have torque capabilities

that fall off at higher speeds. Additionally, the stepper motor requires more power to operate since the coils are energized constantly at maximum current draw. This leads the stepper motor to not be a desired option for the project. The next consideration is the brushed DC motor. These are easy to control with no commutation needed and only a single voltage signal is used to control the speed. The main limitation with these motors is the use of brushes that apply current through the windings as the motor rotates. This is how control of these motors is simple, since the commutation is handled through the brushes and a commutator within the motor. These brushes lead to a couple disadvantages mechanical noise, brush to commutator arcing and wear, brush dust, and a shorter lifetime. For space application these motors are typically steered away from for these reasons and since in a vacuum the lack of a medium leads to stronger arcing. This causes the brushes and commutator to wear out quickly and provides for poor thermal characteristics. The final option for the RPA is a brushless DC (BLDC) motor. These motors operate with less mechanical and moving parts than the brushed motors. Achieved through the elimination of the brushes and having the only moving part being the rotor. Commutation is instead done through electrical signals sent to each winding. With the difference in design, BLDC motors can operate for longer lifetimes, higher speeds, higher efficiency and have better thermal characteristics. These advantages are why these motors, along with stepper motors, are the most predominant in aerospace application. Therefore, the final choice for

the motor type is a brushless DC motor. From knowing the type of motor that works best for the design, research is done to find one that meets the requirements [6].

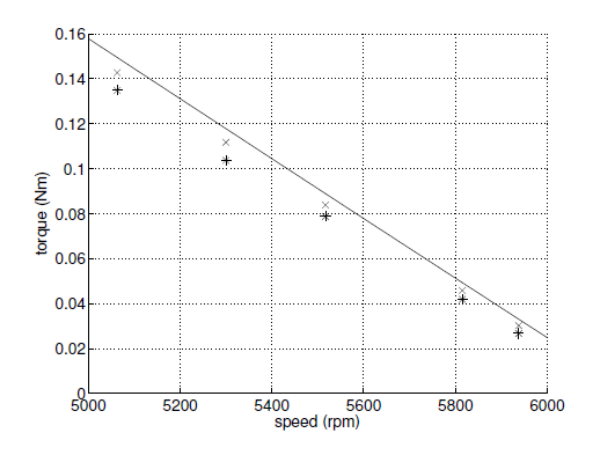


Figure 7: Torque Velocity Example [7]

The first requirement is the velocity requirement, the motor needs to be capable of reaching top speed for scan pattern. At this speed the motor also needs to be able to reach this velocity with the torque load on the motor. Through calculations from knowing torque effects from the motor, bearings, encoder, prisms, and additional loads. An estimated torque load is used to determine if the motor can drive the full system. Then through velocity versus torque graphs supplied from the vendor, the motor is analyzed based off the estimated torque at a given speed. An example of one of these graphs is shown above in Figure 7. For this example, if the top speed the motor was 6,000 RPM then the torque load it can operate at is around 0.02 Nm.

The second requirement is power, the motor must utilize as little power as possible during acceleration and top speed. In order to determine the power that is used for the scanner, a couple of parameters are used. The speed in which the scan happens gives insight into the max voltage that the motor runs at. This is done through checking datasheets on each motor to find the back EMF constant. Since in BLDC motors an

energized stator powers the rotation of the rotor, this causes an induced AC voltage in the rotor. The effects of which are determined through measuring the output terminal voltage of the motor at certain speeds. This measurement is a constant dependent on velocity that is expressed as back EMF. From knowing the opposing voltage of the motor at a given velocity, in order to cause rotation, the motors input voltage is estimated slightly higher based on the constant. For example, if the back EMF constant is $17 \, V/KRPM$ and the motor is driven at $1,000 \, RPM$ the input amplitude voltage needs to be greater than $17 \, V$. To estimate the current on the motor the torque constant is used. From calculating the estimated torque load on the motor, this constant is used to represent the produced current based on the generated torque. Since the motor drives the torque load, an estimated current is derived. For example, if there is a $0.5 \, Nm$ load with a motor constant of $0.15 \, Nm/A$ an expected current of at least $3.33 \, A$ is needed to rotate the motor. Based off these calculations an estimated max operation power of the motor is derived.

The last requirement focuses on the dimensions and weight of the motor. Since the eventually goal of the project is to position the RPA on a lander, these are critical parameters. A large and heavy motor assembly adds weight and in turn fuel cost to the lander. Therefore, when considering the motors, the smaller, lighter sized the better. Additionally, the setup requires the motor to hold the Risley prims and have a laser pointed through them. This requires a special type of BLDC motor called a frameless motor. These operate the same as normal BLDC motors but have rotor and stator components not fixed in a standard motor housing. Meaning they don't include an output shaft or shaft support bearings. Instead where the output shaft normally is there is a hole of a certain diameter. This diameter is dictated based on the needs of the project. The larger

the diameter the more feedback light from the laser is collected. For landers with a low light reflective surface a larger diameter is required and for high reflectivity a smaller diameter is required.

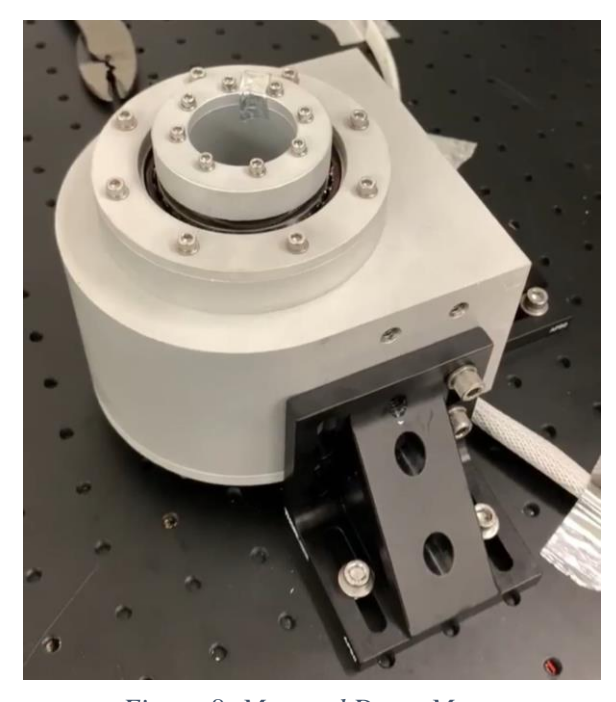


Figure 8: Mounted Demo Motor

From these requirements a couple motors were chosen which met the standards for the RPA design. For the rapid prototype a frameless BLDC WYE configured COTS motor is selected with hall effect feedback included in the stator assembly and temperature feedback through a thermistor. For the demo motor housing was created to fix the stator and rotor in place. Additionally, a couple of L-brackets were used to hold the motor fixed on a tabletop to reduce vibration. The housing was grounded to earth ground to reduce magnetic effects and to insulate the motor. Wiring of each motor was split into two sections, the winding power and feedback paths. These lines were both shielded in a conductive sleeve, that is also wired to ground to prevent electromagnetic interference between the feedback and 3-phase power lines, thus reducing noise. By creating a rotor

cap, the prisms were mounted and glue on the ends of the motor. The final step positioned and mounted both motors next to each other, so the prism were close together. An image of the assembly for one of the motors is shown in the figure above.

A secondary COTS motor is also selected with the same BLDC configuration and meeting the requirements. This motor fit the design of the project closer than the demo motor. With the dimensions and weight being almost half the size. The motor also had lower power requirements at the top speed of the scanner and a zero cogging torque which reduced the torque effects on the motor. Since this motor was a custom design from the vendor it has a long lead time for construction. Therefore, the demo motor that fit the requirements is used in place of this motor. The tradeoff being that the control of the demo motor is based only on hall effect feedback. Instead of spending resources, when a more adequate motor is being built, the encoder selection focuses on fitting the second motor. Utilizing the first motor while the second was being built gave insight into the drives, control, and operation of the full system.

B. Drives and Controllers

After the selection of a brushless DC motor, a drive system is determined. Since the lack of a commutator in these motors requires more complex drive circuity a couple different COTS drivers and controllers are examined. With the progressive advances in machine automation for assembly lines, autonomous robots, and other automated systems there is many new advances in commercial controllers. These systems have already been tested for plastic injection molding, glass printing, labeling machines, and even a virtual reality roller coaster system. To evaluate these systems, the controllers and drivers need to

be capable of operating the RPA under each phase of the procedure and meet requirements.

The main requirement is the ability to operate the BLDC motors with the needed power and control performance for the scan. For this, the power calculations in the motor design section give insight into the needed output drive power. Based on the calculations a driver with the capabilities to provide this power is chosen. For control performance the motors need to maintain the smallest error in terms of velocity and position. This means the drivers update rate and feedback resolution are an important feature. The update rate provides insight into the performance of the control loops in the system. A slower rate may not be able to maintain the precision needed for the velocity and phase lock for the motors. Also, the feedback resolution of the drives is another factor that adds to the error in these parameters. A system with a high interpolation factor and sampling rate is optimal for better control.

From these requirements a commercial controller and two motor drivers are selected. The drivers operate off either AC or DC to power the internal H-bridge circuitry. Then with the control logic, pulsed 120° sine wave commutation is sent to each phase of the motor. Based on the max and min duty cycle of the pulsed commutation the output voltage levels are controlled. This type of commutation offers the lowest torque ripple for the motors and is typical for a higher performance system. Each drive either operates off torque, position, or velocity control. For the initial demo only hall effect feedback is used, and the drive only operates with velocity or torque control. Since the drivers operate and control each motor individually an additional master controller is used. This gives the ability for multi-axis control based on relative position or velocities between the two

motors. Through an EtherCAT connection, with a 4 kHz update rate, the controller can command position, velocity, or torque of each control loop at a given time. Feedback from each driver gives the controller information on the current status of each motor. Then through a program coded within the controller the memory within each driver is updated with the needed value. Details into the control system used for the project and coding are explained in the control section.

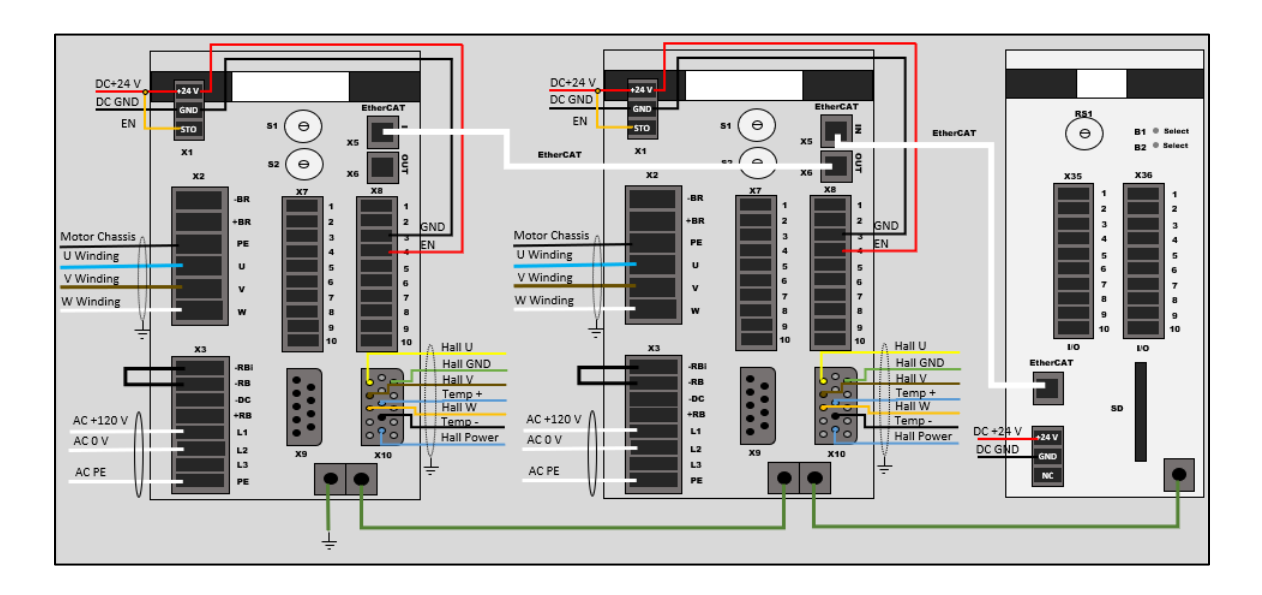


Figure 9: Controller and Driver System

The drives and controller are mounted together in a rack and wired as shown in the figure above. A main 120 V AC line is used to power each of the H-bridges for the drives. An additional 24 V line is used to power the master controller and control logic for the motor drivers. These controllers and drivers are insulated through a chassis ground to earth to reduce electromagnetic interference between them. For communication EtherCAT wires are connected in series between the drives and controller. A network switcher is used to provide connection between the system, router, and computer. Then through either a hard wired connection or remote access the master controller and drives are configured and programmed for the project.

C. Encoder

The selection for the encoder is based on a few requirements and design constraints. For the design, the engineer can base the best option for the RPA on the parameters of encoder type, resolution, accuracy, and dimensions. The output of the encoder is used for position feedback for the motors and as data points for the detector. In order to create a detailed map of the terrain a minimum resolution for the encoder is based upon the needed resolution for the detector. For the maximum resolution the update rate of the control and the maximum speed of the motors for the scan are examined. Since the controller has a given clock rate for the feedback and the motor spins at a certain frequency, the controllers clock limits the maximum resolution. For example, consider the feedback rate of the controller is 1 MHz and the motor spins at 5,000 RPM for the scan. This means the controller reads at a rate of 1 µs while the motor completes a revolution every 12 ms. Using these calculations, the maximum number of samples per revolution is 12,000 then converting the value to a bit resolution the max is ~13 bits. Therefore, using these numbers and calculations, the maximum and minimum resolution of the encoder are determined. The accuracy for the encoder sets the error based on the true position of the motor being measured and the position reported by the encoder. This value does not relate to the resolution of the encoder and is typically measured in arcseconds or microns based on the type of encoder. Since the value represents the error for the encoder, the smaller the value the better.

The next limitation for the encoder is the dimensions and type. Since the BLDC motors for the project are frameless, with the ability to have a laser shined through the center, the encoders cannot block the prisms output. Therefore, the mounting of the encoders is

positioned on the rotor with a bore equal to or greater than the bore of the motor. The size of the outer diameter for the encoder leads to the maximum diameter of the RPA. A smaller encoder leads to a smaller housing which makes the dimensions of the encoder critical. The type of encoder is based on the needs for the prism. Since the absolute position of the prims are needed for the control of the scanner and detector feedback, an absolute encoder is more viable. On the other hand, an incremental encoder bases its' measurement in relation to a starting point. Which means each time the system is turned on a new starting point is used for reference that does not dictate the starting position of the prisms. Therefore, the absolute encoder is the preferred choice for the RPA. The final choice for the encoder is chosen based on the environmental requirements. Since in most space application a general concern is radiation and magnetic interference which adds noise to the system and causes shorter lifetimes. For the project one potential mission is a highly radiate and magnetic environment. Therefore, an optical encoder is of more benefit than a magnetic encoder which would provide for a less noisy signal in an extreme environment. Since optical encoders are still affected by radiation the selected encoder must have rad hard capabilities. The encoder is also mounted in a surrounding housing to prevent additional radiation effects. A final rad hard, absolute optical disk encoder is chosen for the RPA.

V. CONTROL

A. Velocity Loop

In order to control the motors a few things had to be taken care of. The first of which is setting up the motor drivers control loops for system performance. The COTS drive used in the RPA design had a couple different operation modes torque, velocity, or position.

Each had its own unique control loops with filters, PIs, limiters, feedforward, and other control options. These parameters for the drive are edited through user input. An auto tuning function is also available for the control loops but when utilizing hall effect feedback only, the auto tuning is not available. Therefore, tuning of the system is done based off the main criteria, velocity.

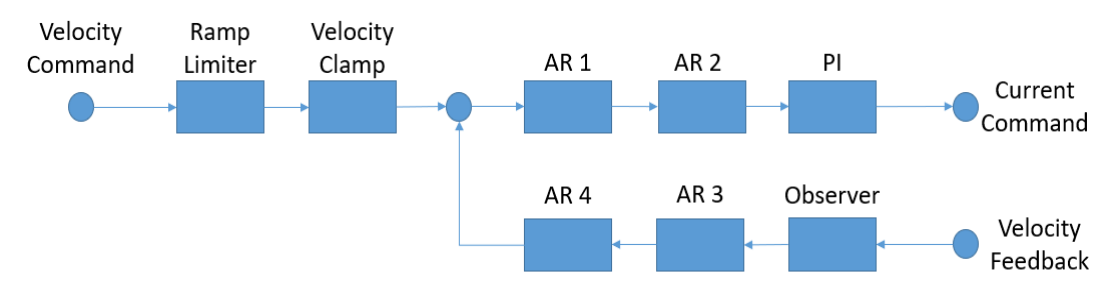


Figure 10: General Control Block Diagram

The general block diagram for the velocity control loop is shown in the figure above. Using the feedback from the hall effect sensors and an ideal velocity command, the control system outputs a current onto the motors to produce movement. Since the hall feedback is heavily quantized, to be used for velocity, large current spikes occur at each transition points. The unedited velocity feedback from the system appears as a series of random impulses due to the current spikes and an exact value cannot be determined. In order to filter the noisy signal an observer and a set of anti-resonance filters, represented by AR, are used. The observer, also known as a state observer, is used to estimate the state of a given system through measuring the input and output of the full system. For example, if a car enters a tunnel the speed and position the car enters and exits are known by the observer. Then from this knowledge an estimated position and speed within the tunnel at a given time can be mapped. In this case, by knowing the input and output current command an estimated velocity is generated from the observer. This signal is filtered within using a low pass filter to reduce the noise before use. After the observer another series of filters

are also need. Each AR is capable of being either unity gain, low pass, biquad, notch, or lead lag. Since the output signal from the observer sill presents noise in the system two low pass filters are added. This provides a clean velocity feedback signal that is then used to determine the error based on the velocity command. First a ramp limiter is used which sets the max acceleration for the motors. The velocity command is then limited by the max output velocity set by the user. Which is determined through max velocity limitations of the motor. A generated error signal is then able to be filtered through AR1 and AR2. A single low pass filter is used to reduce noise in the error signal with a lower quality factor than the velocity feedback filters. The error signal then is controlled through a PI system to produce the current command on the motors. Exact tuning for the PI system is done by hand since the auto tuning function is unavailable when using hall feedback. The performance of the tuning is evaluated through the percent error between the commanded velocity and velocity feedback from the hall sensors. Results of the performance of the control system are shown in the results section of the project.

B. Coding

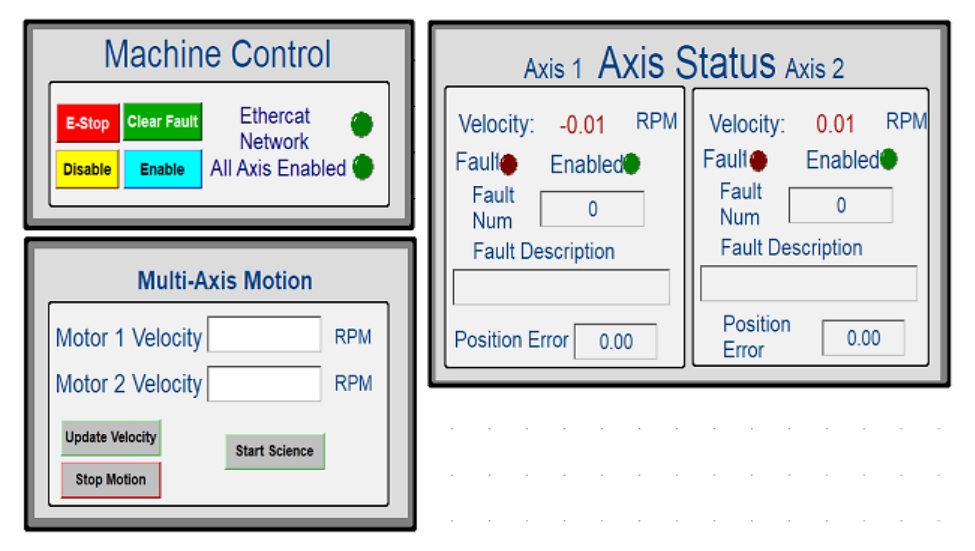


Figure 11: Control Panel

The drives for each motor use the velocity control loop to maintain the desired setpoint, based off the velocity command that comes from the master controller. Using the software for the controller a control panel, with background code, is created. The figure above shows the interface for the user and the software. The control panel allows the input of velocity commands for each motor and provides feedback information on the status of the motors. When the code is run the panel provides the status of the EtherCAT network. Once communication between the controller and the drives is detected an LED is set to green. Afterwards, the user can enable each drive through a button on the panel. Once this is done the drives provide commutation to the motors, locking them in place, and an audible tone is heard from the commutation signal. To provide motion the user can input the velocity of each motor through a text box. Although only one velocity is needed for the scan this gives the option of testing different scan patterns for the RPA. Also allowing for different directions of each motor with negative velocity inputs being counterclockwise and positive being clockwise. After pressing a button to update the velocity a command is sent to each drive's memory for the velocity command parameter.

While in motion an axis status section provides the user with the velocity readings of each motor and any faults detected on the drive. Once the desired speeds of the motors are reached the user can start the scanning processes at any time from the start science button. The scanning process is velocity difference controlled with the first motor holding the same velocity and the second motor slowing to perform the needed phase difference of the prisms.

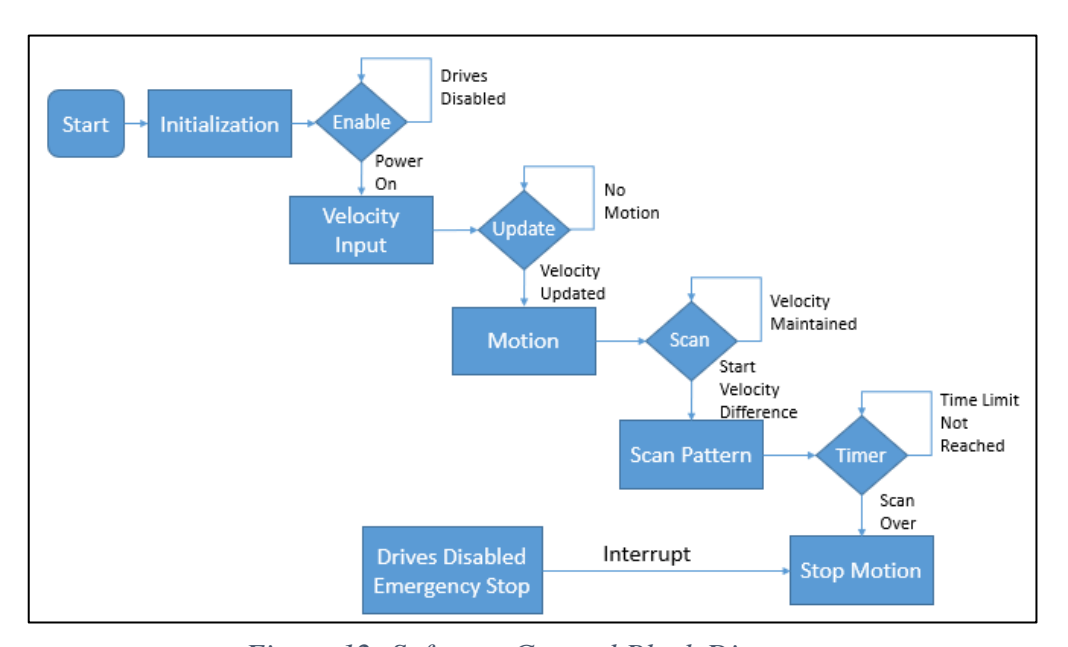


Figure 12: Software General Block Diagram

The control panels input and output variables as well as buttons and LEDs are tied to a background code that controls the system. A general block diagram shows an overview of the process the code takes. For the program three scripts are integrated together, main, triggers, and math section. The main section handles the higher level control like velocity commands, initialization, axis status, and motor readings. Triggers handles the sub level control of timers and flags for the system. Math takes care of data conversion and details the scanning equation in terms of velocity. The first part of the program is initialization, here the motion library for the code is stated for the compiling of the program. Since the

controller can be coded using a couple different languages all unique to the controller.

Once the library is imported into the software the EtherCAT lines are cleared. Each axis is then assigned a variable that can be used in the code, tied to a specific drive. After the initialization the program enters a conditional statement based on the enabling the drives from the user. If the drives are enabled from the button on the control panel, the system enables power to each of the motors. Power is then disabled if the user presses an emergency stop button or disables the drives anytime during the program. In the event of an emergency stop the controls output a breaking reverse current which immediately stop the motors. In any other case the motion is slowed through a deceleration function controlled from the users input.

The code, within main, then comes to two write to memory functions. These functions are set up to write the specific velocity value to the velocity command parameter within the memory of each drive. The value is command based on the EtherCAT slave address, memory index and sub index within the system. This function executes only when the user presses the update velocity button on the panel. The input into the text box on the control panel is converted into a usable value from the math section. Since the memory requires the velocity value to be defined in 1,000 of RPM. Acceleration of the motors is controlled through a parameter defined in the drive's setup.

Once in motion the main code uses two memory read functions to display the value of the velocity feedback parameter within each drive. The function works like the write to memory command using the EtherCAT address and memory index for the value. Since the functions are single executes a clock signal is created within the triggers section of the code. This function outputs a pulse wave modulation signal from zero to one based on the

desired speed of the function. The max clock speed is used to get a constantly updated and reliable value that is output to the control panel for the user. The math section again converts the value to a readable RPM before output.

For the scanning portion of the project the start is controlled from the user pressing the start science button on the control panel. Once this occurs the trigger section executes a timer that measures the elapsed time since the button has been pressed. Through the math section it is converted into a usable variable that can be input into a velocity difference equation. Since the motors for the demo are operating in a velocity mode instead of the ideal position mode, the phase difference equation is converted. This is done through taking the derivative of the ideal position equation to get velocity. Then within the math section, it is created through a series of functions that use the converted time as the dependent variable. To account for system error an additional constant is added to the end of the equation. The value of which is determine through trial and error based on the required scan time. An ideal scan time of a couple seconds is defined by the project requirements, this is the determining factor for the additional error. The output of the equation is the velocity difference between each motor. Therefore, this value is subtracted by the current velocity of the first motor and is output to a new write to memory function. Since these functions are single executes, the clock signal defined in the triggers section is used to continuously update the memory. Once the scan reaches a certain time, input from the user, the triggers section sends a flag to main. This flag then commands each motor to decelerate based on initial setup. When the motors reach no motion the final stage of the RPA has finished.

VI. SCANNER SIMULATION

A. Overview

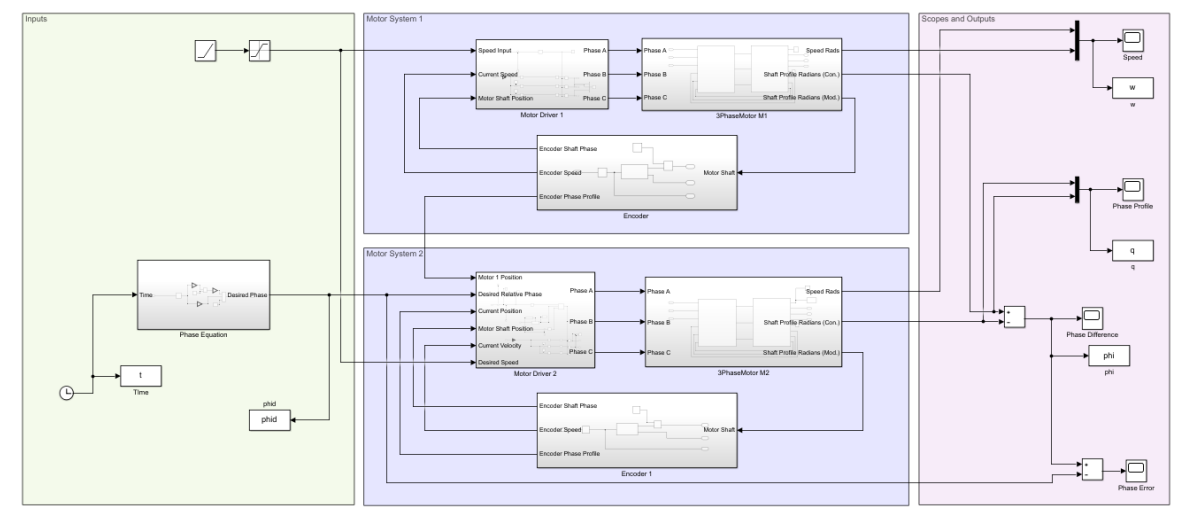


Figure 13: MATLAB RPA Simulation

In order to understand the construction of the scanner, project teams developed a couple simulations. These gave expectations on parameters from the design that aided in construction of the project. For the RPA important information can be determine from simulating the control system for the motors. Some outputs that the simulation provides are winding voltages and currents, torque, velocity, motor phasing and more. Of these the phasing information can be sent to the optical to teams' simulation to helped determine features like pixel per spot coverage. Since the optical simulation provide more information on the detector and laser for the scanner.

The creation of the RPA sim focused on modeling the full system through motor drivers, motors, and an encoder system for position feedback. Utilizing MATLAB, the simulation shown in the figure above is created. The full system operates each of the three phases listed in the procedures. For the first phase the drives are commanded through a ramp function based off the ideal acceleration of the motor. This function is limited through a saturation block to a desired settling speed. The second phase uses a phase

difference input equation into the second motor driver. Then based off the feedback from the first motors encoder, the ideal position is commanded to the second motor. Once a set time is reached, defined by the user, the phase difference equation outputs the motor position over time for the scan pattern. When the scanning period is complete the simulation is ended, and an output of the scan pattern is show to the user. Parameters for the drives and for the motors are controlled through user input from a script file.

Additional outputs are also controlled and collected through the same script.

B. Motor Drivers

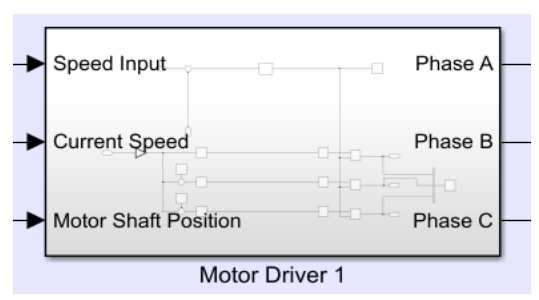


Figure 14: Simulation Motor Driver 1

Two motor drivers are created to control identical motor systems with one being a slave to the other. The first motor drive controls and executes all the steps for the first motor. Inputs for the drive include the desired speed of the scan, current speed of the motor from the encoder, and encoder motor shaft position. With these inputs a velocity control loop is created and a PID system maintains the output voltages onto the three phase motor windings.

To simulate the drives picked during the brainstorm process of the design phase a couple of attributes were used. The first of which is the output of sinewaves to mimic the COTS drives. This is done through utilizing the feedback from the encoders motor shaft position. A quantized and sampled shaft position that when scoped forms a sawtooth

waveform from 0 to 2π . Based on the motors shaft position the drive calculates the needed commutation sequence to move the motors. Typical sinewave commutation uses three signals offset by 120° or $\frac{2\pi}{3}$ radians. Therefore, each phase has an addition of this offset, phase A +0 radian, phase B + $\frac{2\pi}{3}$ radians, and phase C + $\frac{4\pi}{3}$ radians. Using this information, the drive can output commutation for one electrical cycle of the motor. In order to operate a full rotation, the number of poles in the motor is also considered for the electrical cycles. As a gain function, the number of cycles is multiplied by the motor shafts modulated position, giving the drive the ability for complete rotations. The equation (4) below represents how the drives calculate the commutation signal for each phase of the motor. Where SP is the motor shaft position from 0 to 2π , EC represents the electrical cycles, and the values of which are assumed to be radian values. The output of the sin function is a signal that oscillates between zero to one depending on these values.

Phase
$$A = A * \sin(SP * EC)$$
 (4)

Phase $B = A * \sin(SP * EC + \frac{2\pi}{3})$

Phase $C = A * \sin(SP * EC + \frac{4\pi}{3})$

For the sinewaves to produce a voltage to drive the motors, the output of the equation is also multiplied by A, the amplitude of the signal from the control loop. The first motor for the scan, only needs to come up to a velocity and hold. Therefore, a velocity control loop is used to generate the voltages on the motor. Using the desired speed input from the user and the current speed, read from the encoder system, an error function is created through the subtraction of the two. The error feeds into a PID control block that outputs the voltage amplitude. Each PID in the simulation is tuned to a specific need. For motor one the important parameter is velocity. Therefore, the PID is tuned based on quickest settling time and lowest velocity error using a MATLAB auto tuner and additional hand tuning afterwards. To also represent the control system the PID is run in discrete time based off the update rate of the motor drives. Limitations are also set on the amplitude of the output voltage to ensure the output is never more than the driver can supply. Finally, in representing the motor drives, the output commutation is quantized based off the output resolution.

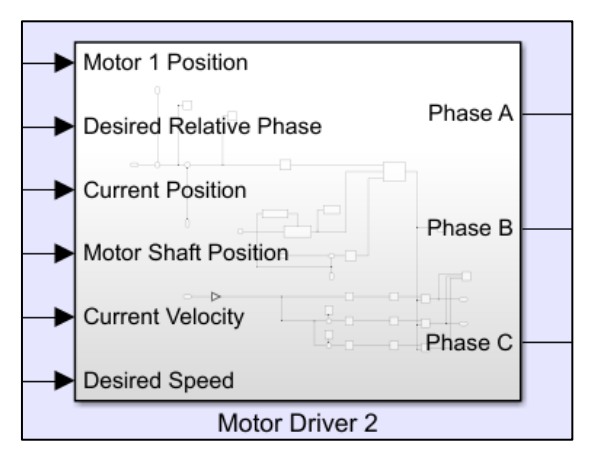


Figure 15: Simulation Motor Driver 2

The secondary motor drive operates differently compared to the first drive since its procedures are more complicated. Motor 2 needs to operate the same as motor 1 during the first phase by coming up to a desired speed. But in phase 2 and phase 3 the second

motor has a phase difference requirement to start and preform the scan pattern. The inputs for the driver are the same as the first with the addition of a desired relative phase and position of motor 1. End goal is again the same with motor shaft position being used to determine the commutation output at a certain voltage. This voltage is determined by two different control loops a velocity loop and a position loop.

During the first phase of the simulation the velocity loop is used to get the motor up to speed. The same PID tuning, update rates, and voltage limits are used as in the first motor driver. An additional trigger is added to switch between this loop and the position loop. Once the speed of the motor is detected to have reached the settling velocity the switch occurs. The time when this is triggered is saved as a variable to be used to know how fast the motors came up to speed. Utilizing a switch between the two loops is done for stability. When the two loops are cascaded, velocity and position, the two functions fight each other and cause oscillation. Additional ringing is noticeable in the second and third phases in the position of the motor. This also emulates the control of the drives which utilize different control loops in order to drive the motors, a position, velocity and torque loop.

C. Motor

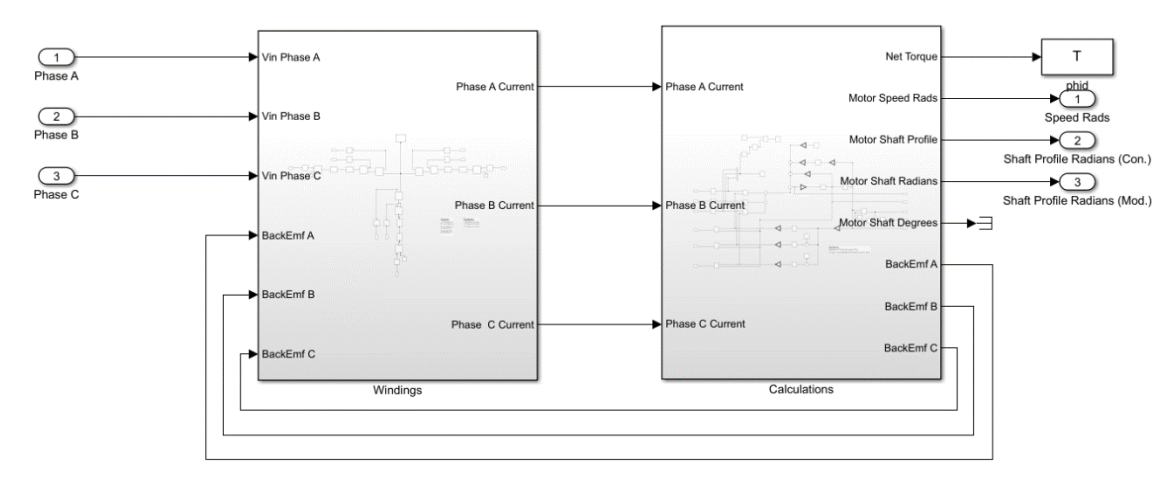


Figure 16: Simulation Motor Model

The motor system for the simulation is controlled by the motor drives through the voltage output commands. This system is split up into two different function blocks, a winding model and a mathematical model that represents the motor. The motor windings input the voltage commutation from the drives, and the back EMF from the math section. Outputting phase currents based on the resistance and inductance of the motor. Which are used to generate motion from the calculations block. Parameters are then calculated from these currents such as motor velocity, torque on the motor, winding current, shaft position and more. Representation of the motor focused on a brushless DC WYE configuration, since it was the optimal choice in the design phase. There are a couple assumptions that are made in order to reduce the complexity of the model. Which are, no magnetic saturation, no hysteresis and eddy current losses, uniform air-gap, no mutual inductance, and no armature reaction.

Each phase of the motor is represented in circuit form within the winding model.

Utilizing resistors for the line to line resistance and inductors for the line to line inductance. These values are divided in half since each phase is modeled based on the line

to neutral form for easier representation in the simulation. A single series resistance and inductor to a zero point serves as one line of the windings. The zero point is a function solver that ensure the neutral point of the motor is always at zero. Then the calculated sinewave voltage is injected across each phase of the motor. In opposition, a back EMF signal generated from the calculation section that opposes the commutation signal. The total voltage across the winding is calculated from the equation shown below (5). Where R represents line resistance, e is the back EMF, i_n is the line current and L is line inductance.

$$V_{a} = i_{a}R + L\frac{di_{a}}{dt} + e_{a}$$

$$V_{b} = i_{b}R + L\frac{di_{b}}{dt} + e_{b}$$

$$V_{c} = i_{c}R + L\frac{di_{c}}{dt} + e_{c}$$

$$(5)$$

A current sensor is used on each of the phases to measure the value of the line current. The measured value is sent to the calculations section to determine the generated electromagnetic torque of the motor. This is done through utilizing the back EMF constant since in practice it is equal to the torque constant of the motor. The torque constant of the motor is given in Nm/A and describes the relationship between the motor current and generated torque. By multiplying the constant times each of the phase currents and summing the results, the total torque is found. This is done in the form of back EMF that is re-injected into the windings of the motor and additional information is shown later.

The generated torque of the motor is then used to determine the acceleration, speed, and position of the motor shaft. On the motor there is always an opposing torque that is

represented through a subtraction function from the generated torque. Here parameters such as viscous damping, bearing friction, cogging torque, and static friction are represented. The static values are simply created as addition to the applied torque on the motor. Values like viscous damping are created through a gain function based off the speed of the motor since it is a function of velocity, viscous damping = Nm/RPM. For cogging torque, the function depends on the position of the motor and represents the effects between the rotor and stator slots of the permanent magnets within the motor. By multiplying the motor shaft position, electrical cycles, and putting it through a sin function the position of the cogging is calculated. Then through a gain function the cogging torque value is represented from the multiplication of the result position. These values are all summed together to oppose the generated torque and the subtraction forms the acceleration torque.

$$Acceleration = \frac{Generated\ Torque-Opposing\ Torque}{Inertia}$$
(6)

Through the following equation above (6), the acceleration of the motor is calculated utilizing the inertia, generated torque, and torque on the motor. From the calculated acceleration value, the speed and position are also determined by taking the integration of each value. For acceleration the integration brings velocity, and from velocity the integration brings position. The output of the position function is a continuous phase profile. For the variable to be used as the motor shaft position the output is modulated from 0 to 2π . The speed is also output from the model and is used in the viscous damping and back EMF calculations.

The last part of the calculations section is to generate a back EMF voltage across the motor and for the torque generation. Since the back EMF signal is controlled through position the output from the integration of the acceleration is used. This value is multiplied by the electrical cycles for position and passed through a sine function. For commutation each phase is offset by $\frac{2\pi}{3}$ radians and then multiplied by the back EMF constant. To generate back EMF the output is multiplied by the current speed of the motor. Since the constant is given in V/RPM the final output is a voltage that is sent to the winding model. To generate the torque from each phase current, instead of multiplying by velocity to get back EMF, the function is multiplied by each phase current. The following equations (7) (8) show how each of the functions are calculated where the first three are for each back EMF per phase and the last is the torque generated. The F(x) represent the sinewave function generated in the model, e is the back EMF voltage, ω is for velocity in rads/s, t is for current, and K_e is for the back EMF constant.

$$e_a = K_e * F(x) * \omega$$

$$e_b = K_e * F\left(x + \frac{2\pi}{3}\right) * \omega$$
(7)

$$e_c = K_e * F\left(x + \frac{4\pi}{3}\right) * \omega$$

$$T_e = \frac{e_a i_a + e_b i_b + e_c i_c}{\omega} \tag{8}$$

D. Encoder System

The modulated output from 0 to 2π of the motor shaft position is further used in the control system. An encoder model is created to represent a simulated encoder based off specifications from the design. For this encoder, the modulated shaft position is quantized

based on the resolution of the encoder. Additional quantizing is also added here based extra interpolation from the motor drives or an extra interpolation box. To also represent the drives after quantizing the position the value is also sampled at the rate of the drive. This allows the system to output values that are closer to the actual encoder. Three outputs come from the encoder system an encoder speed, encoder shaft phase, and an encoder phase profile. The encoder speed represents the calculated velocity that feeds directly into the drive for the velocity control loop. The phase profile is used to make a continuous representation of the position of the motor and is used to feed the second motor driver as a slave. The last output is the encoder shaft phase which is a modulated and quantized position that is feed into the drive. Used to calculate the commutation in order to drive the motors.

E. Phase Equation

The last part in the control model simulation is the phase equation for the Risely prisms. It is used to determine the ideal phase difference of motor one to motor two and is needed for phase one and phase two of the scan procedure. The module works through a cubic equation formed form a series of MATLAB blocks. A time variable is used as the input to pass through the equation which represents the passing time of the simulation. The time variable is first delayed by an amount of time set through user input. This delay marks when the RPA starts the scanning process. Before the delay, the time variable is zero and only the constant of the cubic equation is output. The constant represents the phase difference needed for phase two of the RPA project. Which is used when the motors reach the desired settling time and the switch of the second motor driver is triggered for the position loop. After the set delay time from the user the phase difference equation is

initiated and the time passing through increases from zero. The cubic equation then outputs the ideal phase difference to perform the scan. After a couple of seconds or a time defined by the user the simulation stops and the scan pattern and other outputs are displayed.

F. Simulation Script

Behind the MATLAB simulation model there is a control script that is used for variables and outputs. The user can input parameters regarding the brushless motor like back EMF, line resistance, line inductance, viscous damping, and others. Additional, parameters for the other aspects of the simulation like science start time, encoder resolution, driver limits, acceleration limits, desired speed, and more are defined here. After the initialization of these variables the script runs the MATLAB Simulink model for the RPA. Then through a series of MATLAB functions certain parameters like speed, phase profile, phase difference and more are output in graphs once the simulation is complete.

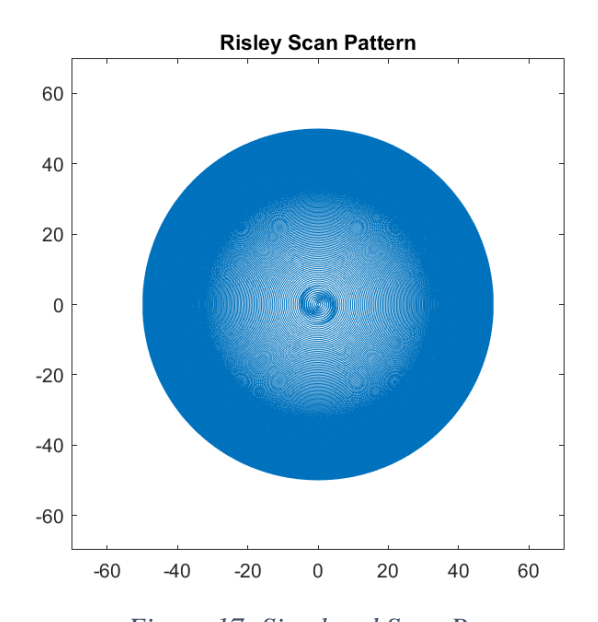


Figure 17: Simulated Scan Pattern

From these the user can determine the performance of the system. With the speed graphs the output shows if the motors reach the desired speed and how long it takes them to settle. Phase difference is used to determine how well the motor controls follow the ideal equation. An error graph is also used based of the same variable. The final output of the script is a scan pattern that is mapped onto a graph. An example of the output of the graph is shown in the figure above. To create this pattern the general equations from the Risley prism section are used. Based off the phase difference of the prisms and refraction angle the X and Y positions of the laser are calculated based on each prisms effect. To represent the scan pattern taken through both prisms the arctan of the addition of the X's and arctan addition of the Y's give the final output position of the laser. To represent the additional features like altitude of the lander the final X and Y positions are multiple by the height. Then by using the ideal scanning area to form the limits of the graph the points are mapped on to an area of this size. For example, the graph of the scanning pattern above represents a scan taken at a height of 500 meters with a scanning area of $100 \ m^2$.

G. Simulation Graphs

The following graphs shows a couple of the outputs that are taken from the simulation. The first figure represents the velocities the motors take druing the startup and scanning phase. Each graph represents the different motors based on color, blue is for motor 1 and orange is for motor 2. The second figure shows the velocities the motors take during just the science or scanning phase of the project. The third figure represents the error from the desired phase difference equation and the actual phase difference of the motors. The final figure shows the phase voltages output to the simulated motor with each phase shown in a different color. These are a few of the graphs that are taken from the simulation.

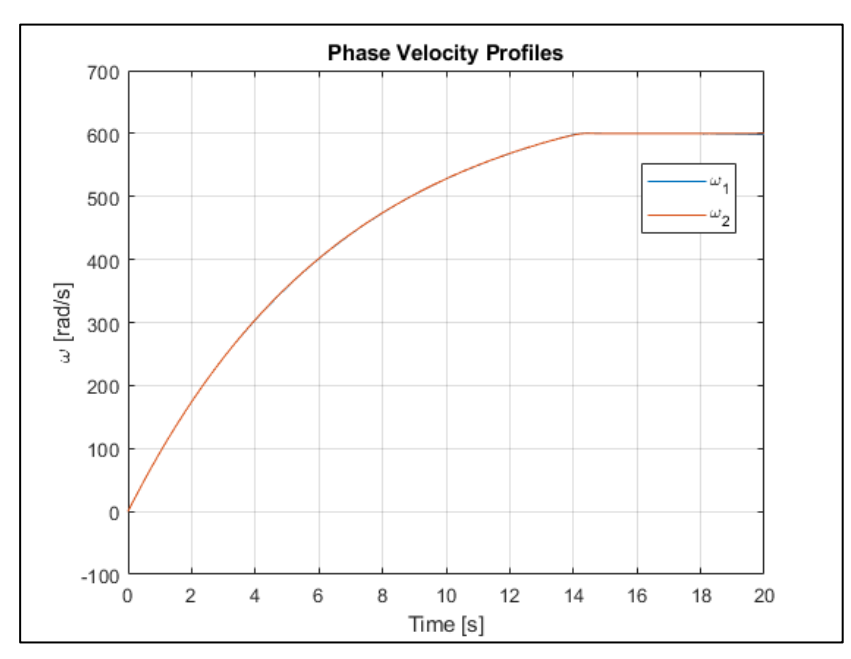


Figure 19: Motor Simulated Velocity Profiles

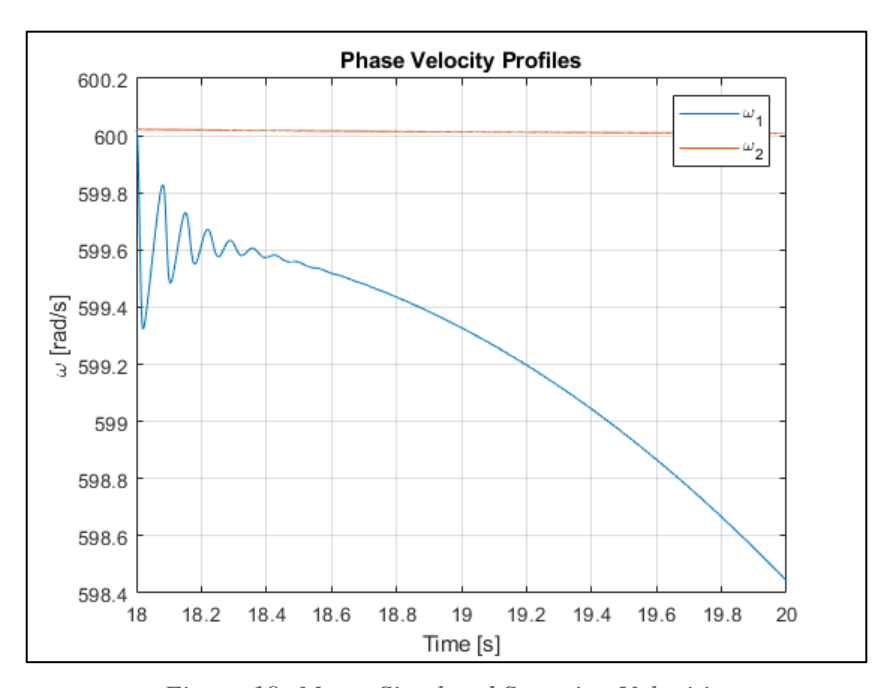


Figure 18: Motor Simulated Scanning Velocities

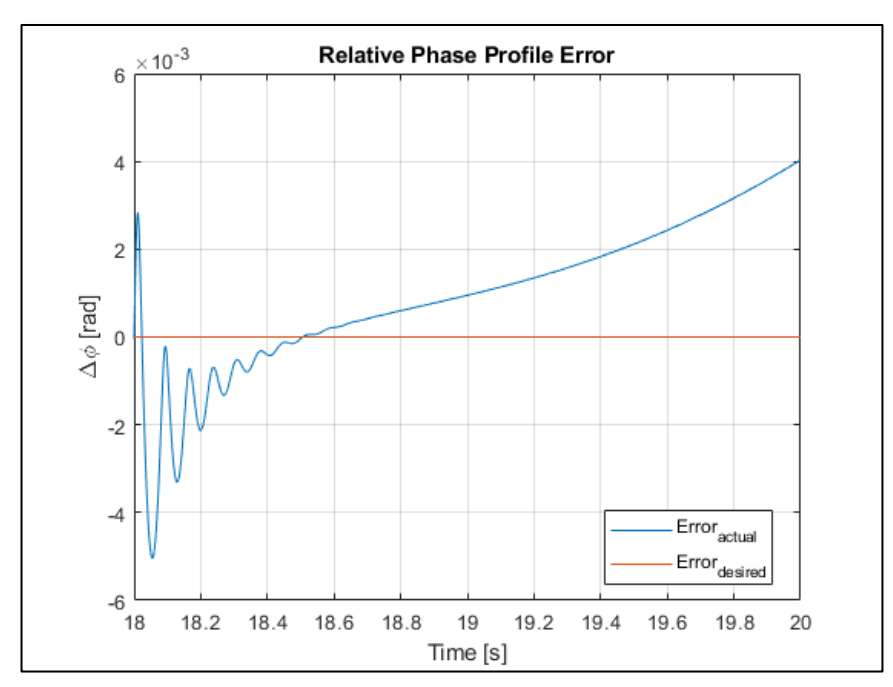


Figure 21: Simulated Phase Error Profiles

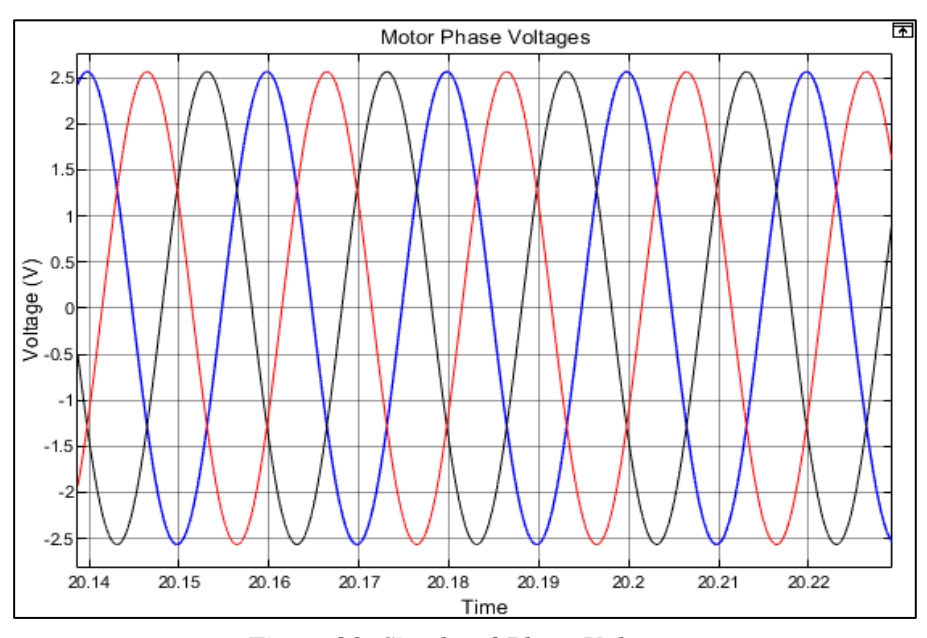


Figure 20: Simulated Phase Voltages

VII. RESULTS

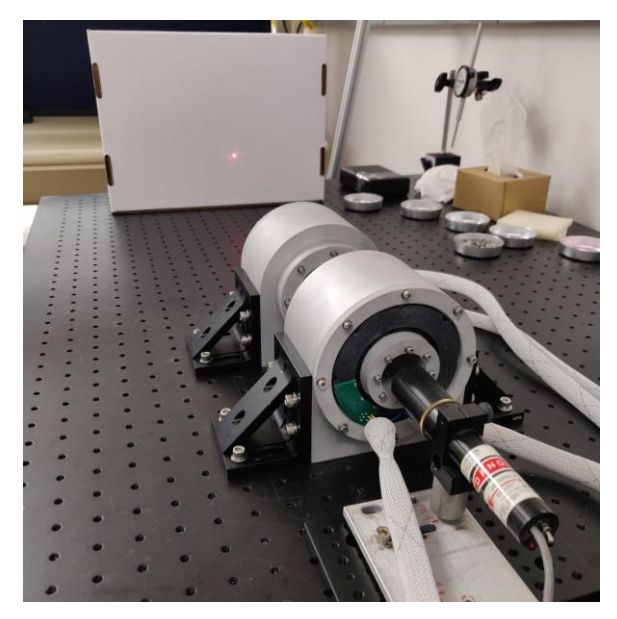


Figure 22: Full System Setup

An image of the full system created by the RPA team is shown in the figure above. For the tests the two motors are mounted using L-brackets to the table. Each is position so that the prisms are as close together as possible without touching during operation. A continuous red laser is also mounted to the table and positioned at the center of the bore for the motors. For the target a white box is used to see the scan created by the laser. An additional box wrapped with aluminum tape is also created to test the pattern. Since the scanner has the potential to be used for a highly reflect terrain or low reflected terrain. To view the pattern long exposers were taken to determine area coverage.

The drives and controller provided software scopes that read parameters from the system. For the drives, the scope gave information on aspects of the motor like winding currents, torque, velocity feedback, and others. The controllers scope had less capabilities since it only reads from the EtherCAT communication line. Therefore, less parameters

were able to be recorded but the additional data came directly from each drive. Using this feature the RPA is evaluated based on the requirements of the project.

A. Performance

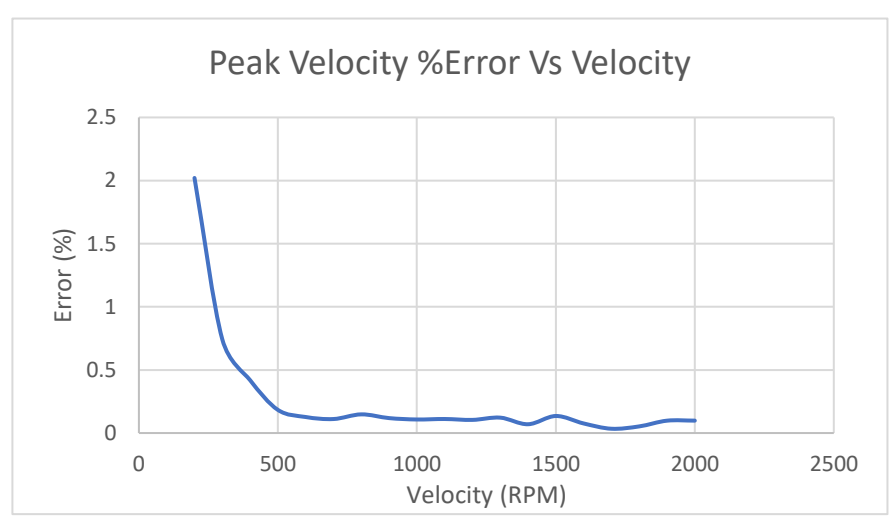


Figure 23: Velocity Error Vs. Velocity

To measure the performance of the system a couple of parameters were evaluated based on the requirements of the project. Since the demo build used hall effect only feedback, the main parameter to create the scan is velocity instead of the ideal position. Therefore, the first criteria examined is the velocity control of the system. The velocity control loops within the drive affects the overall performance to maintain a given velocity set point. As mentioned in the controls section the loop is tuned to give as little error as possible. Utilizing the scope within the drive the parameter of velocity feedback can be graphed versus time. Each measurement is taken within a couple second time period which is the same as the scan time of the RPA. Using the scope, average, maximum, minimum, RMS, and peak to peak values are recorded. For the velocity the maximum error represents how well the control system maintains the commanded velocity from the controller. The following graph above shows the performance of the control loops in an error percentage versus speed.

The graph represents the maximum percent error per each velocity reading. A series of input velocity commands were given to the drives and the feedback was measured after the motor reached the final speed. Using the maximum reading, a percent error is calculated based on the ideal velocity. At higher speeds the control system can maintain the desired velocity at a maximum percent error less than 0.5%. At lower velocities the control system has difficulties maintaining the same rate. This is due to the use of hall effect only feedback. Since the resolution from the three hall effect sensors is too low to give an accurate reading from the motors at low speeds. The controller company provides an estimate from a manual for how low the system can maintain the same rate of speed using this feedback. For example, the drives receive a new position by the hall effect sensor every 60° based on the electrical cycles of the motor. A motor with 6 pole pairs per revolution is 3 electrical revolutions, which leads to a hall position every 20°. This is a low resolution that provides difficulties for the drives. From the manual the limit on control comes from the hall effect frequency and motor poles. For the system used in the project the limit on control is found to be about 250 RPM utilizing hall only feedback. This is seen from the graph where the error rate around 250 RPM is close to 2% and after increasing speeds the error percentage drops. When running the motors at a velocity lower than this the revolutions are no longer a clean rotation and jerk. The measurements taken provide information on the performance of the control system and validate the limits for velocity control using hall only feedback.

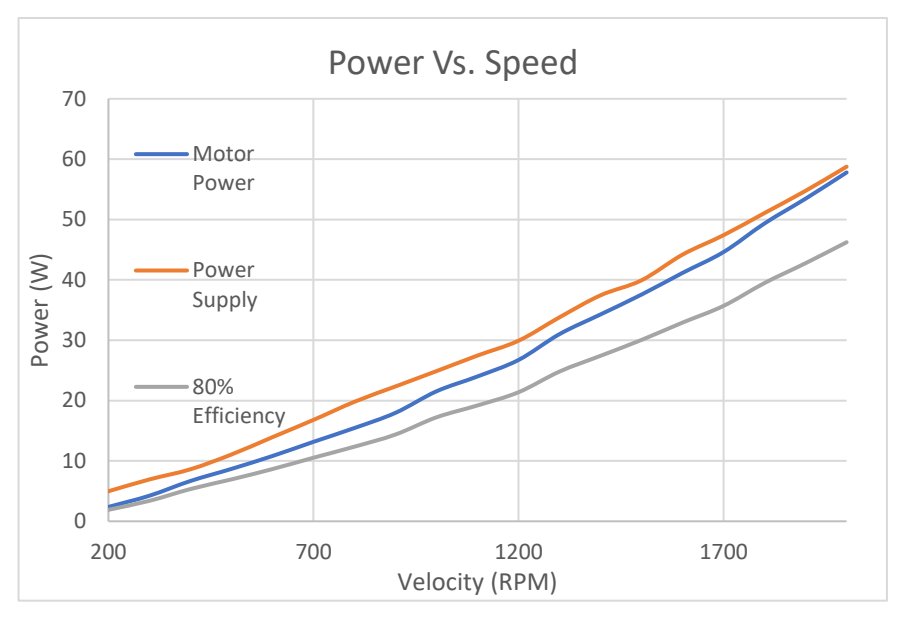


Figure 24: Power Vs. Speed

The second important requirement for the system is power. In order to measure the power consumed by the drives and motors a DC power supply is used in place of the 120 V AC supply. This makes it easier to measure the power consumed since the DC power supply displays the voltage and current usage. The graph above represents the power used over a series of different velocities for a single motor. Since the motor accelerates to reach and maintain a certain speed. The series of measurements give information on the power used for startup and final speed. In the orange the recorded readings come from the DC supply, blue is an estimate from the motor windings, and grey is an 80% efficiency estimate from the motor. The difference between the motor power and power supply give insight into the efficiency of the power supply. From the graph it is seen that the difference between the supply and motor are generally consistent.

For the motor power, the winding currents and voltages were measured. The drives scope allows for the winding currents of each phase of the motor to be graphed. Each measurement is taken over a couple second time period and recorded to a CSV text file.

To validate the measurements taken from the drive an additional external current probe is used. The probe measured the current on a single winding and the scope results are compared to the drives scope. The values of each matched and for simplicity the data taken from the drive is used. Since it provides information on maximum, minimum, RMS, peak to peak and more.

To measure the winding voltages a single phase of the motor is scoped from an external oscilloscope. The drives output 120° sinewave commutation in the form of pulsed sine waves. Therefore, the oscilloscope displayed a series of pulses at a frequency around 8 kHz that ranged from pulse or minus the H-bridge supply voltage. To determine the actual voltage on the windings the scope probe measures from neutral to a single motor line. This is done through using the DC power supply ground as the reference point. Then using the scope, the maximum and minim duty cycles of the pulsed train give the value of the voltage on the windings. For example, if the H-bridge is powered by 100 V the pulses would have an amplitude equal to this value. Then at a certain speed the max duty cycle is measured to be 52% and the minimum is measured at 48%. A peak voltage of 52 V and minimum voltage of 48 V is calculated, the difference of which represent the peak to peak voltage of 4 V on the winding. This value is then used along with the current readings to determine the power the motor uses. It is also converted to phase voltage since the measurement represents the line to neutral voltage.

The power calculation is based off the total three phase power since it represents the total power supplied to the motor. The value at each speed is graphed and displayed as the blue line. These values assume that 100% of the voltage and current measured are directly used to rotate the motor. Most BLDC motors in practice are not 100% efficient and have

specific efficiency curves that average between 70%-85%. The value of the efficiency changes depending on speed and typically increases as velocity increase until a certain point. After the maximum speed is reached the efficiency drops off as speed increase past this point. To give an idea of the actual power being used to rotate the motor an 80% efficient power is also graphed in grey. Although for the final power measurements the important value comes from the DC supplied power. Since it represents the total power used for the system including the losses.



Figure 25: Long Exposer Scan
Pattern

The last and most important requirement for the RPA is the ability to create the scan pattern. For the prototype there is a couple differences versus the ideal pattern. In order to control the motors with the hall sensors, the pattern is created through a velocity equation. Additionally, the laser used for the project is a continuous laser rather than the discontinuous pulsed laser that will be used on the final system. This provides for a pattern made up of lines rather than dot points. The figure above shows the pattern created from the prototype RPA system using the velocity equation, taken from a long exposer.

From the image, the long exposer gives an approximate reading on the coverage of the scan. Using the continuous laser provides knowledge on the areas within the pattern that

are being traced. This is seen from the differences in brightness of certain spots verses others. An area with a high brightness demonstrates a position that has been covered multiple times during the scan. In reverse the lighter areas show spots where the scan did not cover as well. If the system uses a discontinuous point laser the dots recorded would be more concentrated in the brighter areas. From the figure the pattern shows that the scan covered the full area but performed better at certain parts. At the edges of the circle the scan covers the outside edges multiple times, but halfway through the scan there is a section much lighter than the rest. This means that the scan pattern is working but needs improvement to better cover the full area. Ideally the brightness of the circle would be consistent throughout the full scan showing an even scan coverage.

In order to provide more accurate evaluations on the coverage of the scanner there are a couple of ideas. Using the continuous laser and a long exposer camera the image of the scan created can be turned into a heat map. Utilizing an image processing software, like MATLAB, the image above could be turned into a heat map based on the intensity of the laser. This would provide for an easier way to visualize the area covered. Although a long exposer of the scan can be used to determine performance. It lacks on giving information on the exact points that are missing from the scan. Another possible test is using photo detectors along with a discontinuous laser to determine the positions hit. A series of detectors can be aligned in a target area and the triggered detectors can be measured and recorded. Once the scan is completed the detectors give information on the points hit. For the next stage in the project, using an encoder with a different motor, the encoders position information will be used to compare with the ideal phase equation. This will be the main

test to evaluate the system other than combining with the optical team's detector and laser system to find exact spot per pixel coverage for the full system.

The RPA also had the capabilities to perform other scanning patterns. These are based on the velocity inputs from the user and relative velocity differences between the motors. Using the equations from the prism section there are expected patterns based on the velocity relationship of the prims. From this the performance of the system is also checked on the ability to create the other patterns. The well-known patterns were also able to be created with the RPA and were compared to the expected mathematical patterns. A small difference in the system versus the equations are the direction of rotation to create the patterns. The prisms are positioned opposite as to the positions shown in the Risley prims section. Which makes the maximum angle of diffraction at Figure 4 (c) instead of (a). The difference also makes the relationship to create the patterns opposite in terms of clockwise and counterclockwise rotation of the motors. An expected relationship of $+\frac{\omega_1}{\omega_2}$ is later found to be inversed as $-\frac{\omega_1}{\omega_2}$. Therefore, the input velocity differences are adjusted accordingly to create the expected scan patterns. After this change the RPA preformed all the capable patterns documented from Risely prism systems.

B. Simulation Comparison

The final performance of the system is used to compare against the simulation. Since the simulation is a representation of the physical model the values of each should be comparable. For the project the main parameters come from the requirements of the deisgn. In this case the power to drive the motors, and performance of the control system are the important criteria. The project utilizes a different method of control from the

simulation in terms of feedback. While the project uses hall effect feedback to determine velocity the simulation uses an encoder to determine position. Therefore, when comparing simulation to the model the closest feauture for comparision is power, and the control performance is not considered for this build. Once an encoder system is attached to the RPA the control of the system can be analyzed. By using the position feedback information during the scan pattern and comparing it to the simulations position. This will give a more accurate reading on the comparision between the two.

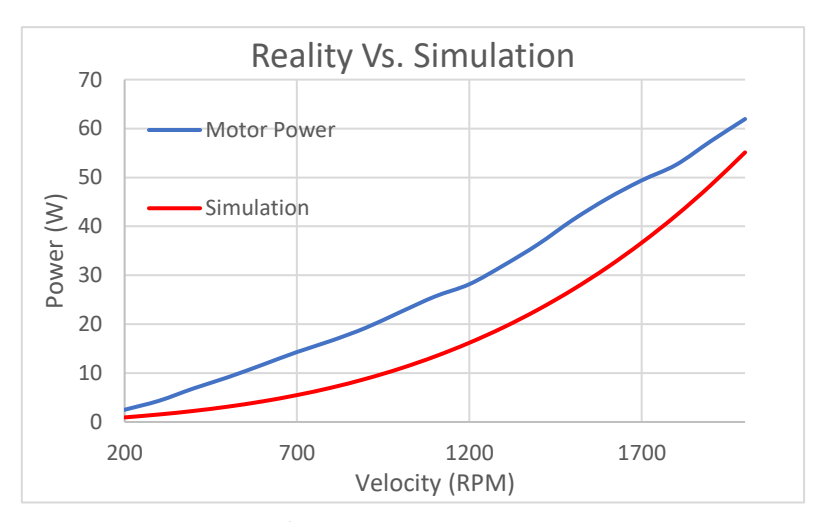


Figure 26: Reality Vs. Simulation Power

The graph represents the three phase power taken from the motor windings. The blue line shows the data taken from the physical model and the red line is the initial simulation. It is seen from the data that the values taken from the simulation are on average less than the physical model. This is expected since the model represents a 100% efficient motor while the physical model has losses from the windings, eddy-currents, magnetic hysteresis and other effects. To reduce the computational load on the simulation these values and efficiency effects were ignored. Another factor that leads to the differences in power measurnments is the commutation method. While the simulation and real system use the same 120° sinewave commutation, the creation of these signals are different. The physical

model uses pulses to create the sinewaves while the simulation uses quantized sinewave signals. Again, this difference is done to reduce simulation run time. Since pulsed sinewaves at the frequency of the drive in simulation cause a large computational load from the numours zero crossing points. The tradeoff leads to a motor with a more efficient drive method than the physical model. The initial simulation also uses values taken directly off the data sheet. These values also have a $\pm 10\%$ variance range with some even having $\pm 30\%$ range like the inductance of the motor. For the simulation the nominal values were used but the actual value could be up to 30% larger.

The last possible issue in the simulation is the representation of the torque. Examing the power curve, the simulation presents a steeper exponential increase when compared to the physical model. This effect come from the viscous damping of the motor and the back EMF. The viscous damping adds torque to the system based on velocity, represented as $\frac{Nm}{rad/s}$ and back EMF is the increase in voltage per velocity as $\frac{V}{rad/s}$. If the visous daming function is set to zero the motors current naturally increases over time from the back EMF constant and increasing velocity. Adding the viscous damping function, increase the needed generated torque to rotate the load and inturn increases current. These two effects are both based off the velocity and create an exponential effect for the current.

In order to validate the simulation the torque on the motor is examined. From the drives the winding current of the motor can be scoped and converted into generated torque based on the torque constant. The current on the windings also includes effects from losses on the motor. In turn the load torque of the system can be calculated from the generated torque. By using the equation in (5), from the simulation section, the loaded torque relates to the generated troque through intertia and acceleration. Therefore, to validate the

simulation and determine the cause from the differences in power, a new loaded torque is created. To ensure the best match with the simulation values and the values of the RPA measurnments from the project are taken. The line resistance and inductance of the motor are found from an LCR meter. Since additional wiring is connected to the ends of the motor the values are slightly larger than the datasheet provides. For the back EMF value an additional motor is connected to spin the rotor of a second motor. Then by measuring the voltage across the windings at different velcoities an exact back EMF constant is derived. The only parameters that were not exact for the system are the torque effects from the motor, from the load, and interia values. These values are taken from the motors datasheets and additional torque effects are estimated from the generated torque. After these measurnments are recorded the updated simulation is tested in the same manner as the RPA.

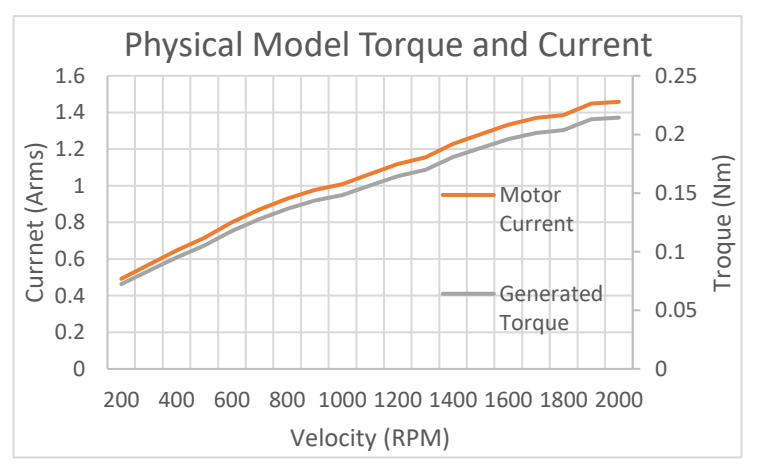


Figure 27: Measured Winding Current and Generated Torque

The graph above represents the current on the windings and generated electrical torque from the current. The values are taken from the drive scopes and converted into torque based on the torque constant or back EMF. Using these values, a linear best fit approximation is made from the torque versus velocity curve. The equation of which is

based on a static torque value added to a linear torque function based on velocity, $T_{load} =$ $t_{linear} * V + t_{constant}$. Where t represents the added torque load and V represents the current velocity. Since the torque load on a motor does not continuously increase over time and reaches a constant load, the function is saturated after a certain point. The saturation ensures that the additional torque is not added to the system and fits the data. From correcting the torque load on the motor, the updated power graph is shown in the figure below. The new curve matches the power curve taken directly from the windings closer than the original simulation. If the loaded torque fit the exact data taken from the drives, the curves would match perfectly. Therefore, the issue for the simulation is accurately representing the motor parameters, load torque and effects from efficiency and losses. Additionally, the current, voltage, and generated torque graphs, are shown below. From the voltage graph after measuring the exact back EMF value the voltage amplitude closely fits the physical model. The corrected parameters have a lower percent error than the initial stimulation. After the correction the average current error is approximately 7%, voltage errors are 6%, and the average three phase power error is 10%.

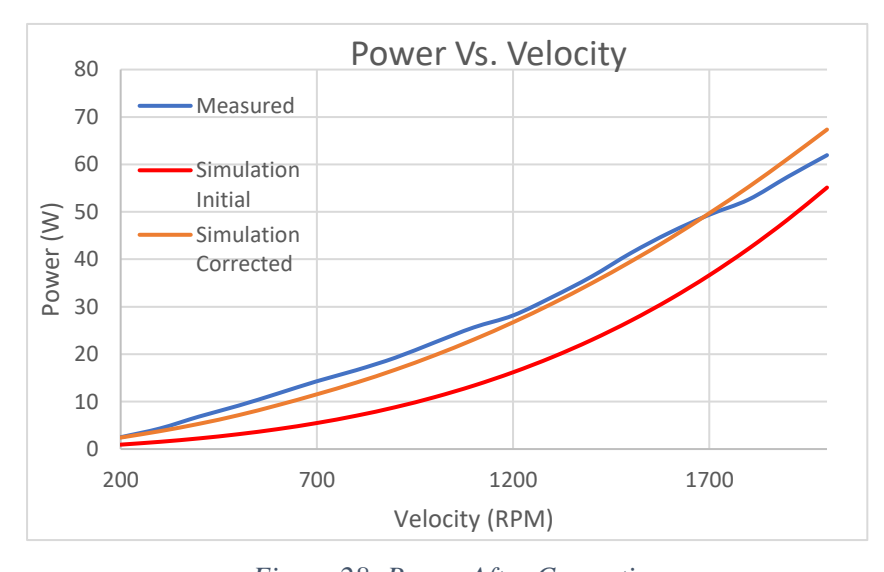


Figure 28: Power After Correction

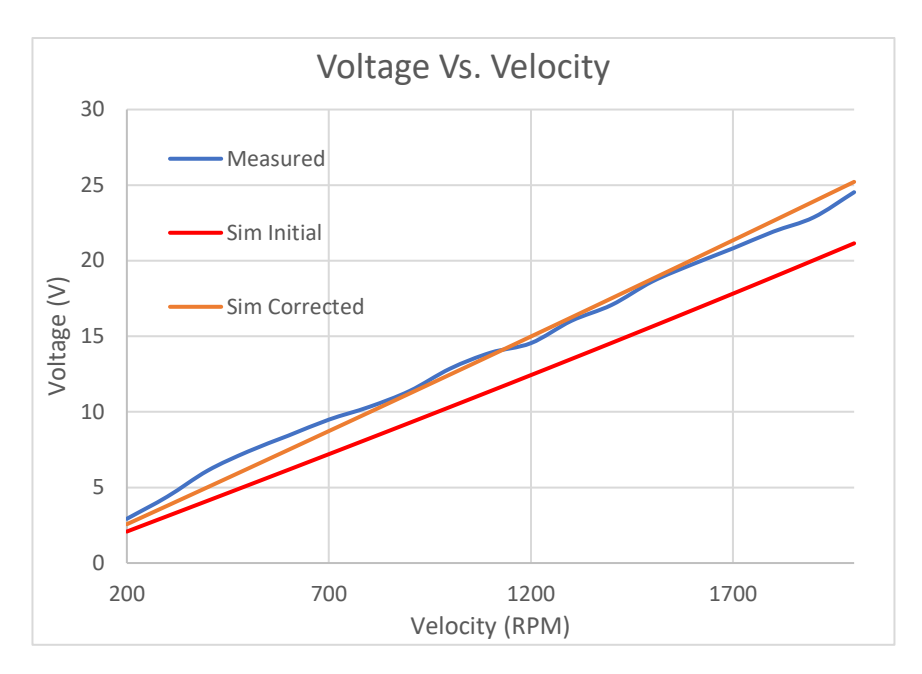


Figure 29: Voltage After Correction

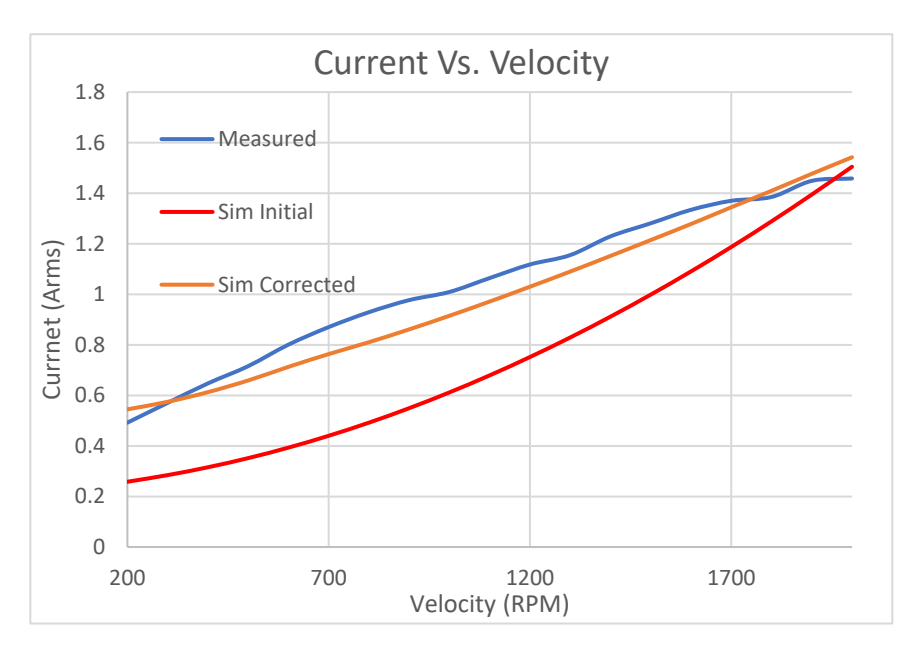


Figure 30: Winding Current After Correction

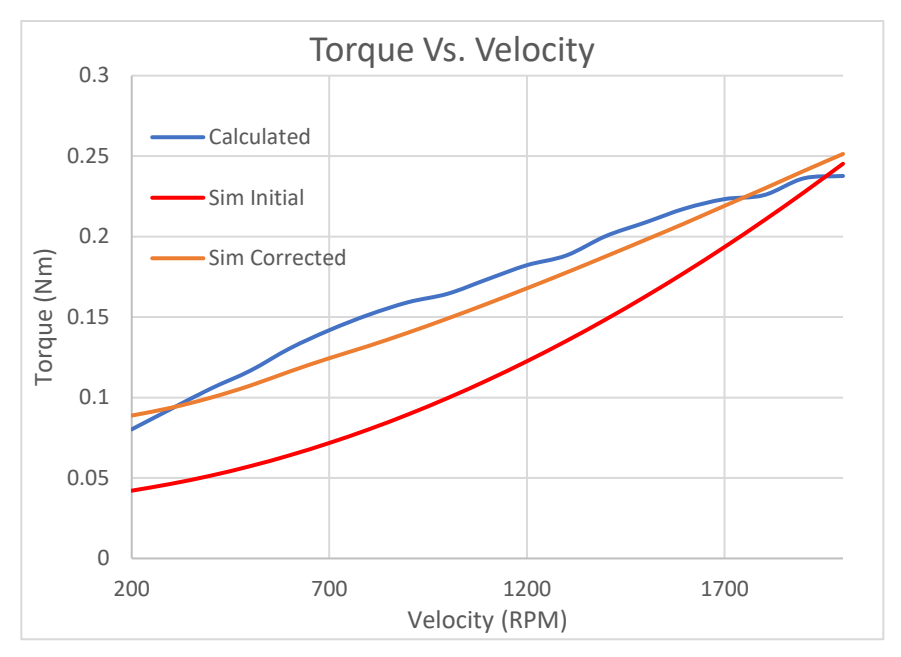


Figure 31: Torque After Correction

VIII. CONCULSION AND FUTURE WORK

The paper represents the work that has been done to build a prototype scanner for the RPA. Detailing steps in order to create, control, and simulate the design. The demo presents insight into the control performance of the system, power requirements, and the ability to create scan patterns utilizing COTS parts. For an initial demo there is still advances to be made in perfecting the scanner system and matching the simulation closer to reality. The next stage in the process is acquiring the encoder and the second motor, which better fits the constraints of the project. These new parts are to be tested utilizing the current controller and drivers to understand the power and control requirements. With the addition of an encoder, position information during the scanning process can be obtained. Giving the capability to accurately see the differences in position versus the ideal position equation. During this time noncommercial options are explored for the driver and controller. Since the branch at NASA has previous experience with 2-axis

motor systems, a controller and driver card have already been designed. These cards have heritage with spaceflight systems such as GEDI. Modification are needed like upgrading max power capabilities, control processes, encoder communications, and others, in order to repurpose the board for the specific project.

The simulation for the project is continually being updated based on the design and data taken from the RPA. The difficulty comes from representing reality versus a mathematical model. Since the exact effects of the physical model are not always known and are approximated. By recording values like voltage, current, position, and velocity, taken from the project, comparisons between reality and simulation are derived. This information allows for the model to be updated and improved for future use. Once a secondary motor system is created the values from another motor can also be compared. With the new system the position information will be recorded from the addition of the encoder. Which will allow for the comparison on the control system performance. The 2-axis motor simulation once refined can be used for other projects and applications. Since motor control is a large part of the electromechanical systems branches' focus.

Lastly, there are many tests before a fully capable flight design is created. Each part is evaluated for operation and performance in an environment like the missions. For example, to test the conditions on takeoff, vibration tests are carried out on the instruments. Additionally, vacuum, thermal, cryogenic, and full system flight tests may be required. For the full system test initial evaluations can be done through helicopter flights or rocket landings. Mounting the system to the bottom of a helicopter allows for taking scans at different heights and terrains to measure performance. In order to simulate a more realistic flight test the scanner has the potential to be mounted on a rocket. A possible test

launch is schedule with Blue Origin which has already demonstrated a successfully launch and landing of a rocket called New Shepard. After the completion and successful operation of these tests then the scanner is available to be used for a spaceflight mission.

IX. REFERENCES

- Robert, Duncan C., et al., editors. Proceedings of the Apollo Lunar Landing Mission Symposium, June 25-27, 1966: Apollo Navigation, Guidance and Control. Manne Spacecraft Center Houston, Texas 1966.
- "InSight Landing Press Kit." *InSight Landing Press Kit*, California Institute of Technology, Nov. 2019, https://www.jpl.nasa.gov/news/press_kits/insight/landing/.
- National Aeronautics and Space Administration. "Space Technology Game
 Changing Development SPLICE: Safe and Precision Landing-Integrated
 Capabilities Evolution" Fact sheet. FS-2018-07-292-LaRC. Lyndon B. Johnsons
 Space Center. Houston, TX. n.d. Paper.
- Schwarze, Craig R., et al. "Risley Prism Scan-Based Approach to Standoff Trace Explosive Detection." Optical Engineering, vol. 53, no. 2, 2013, p. 021110., doi:10.1117/1.oe.53.2.021110.
- 5. Thorlabs, Appl. Note Risley Prism Scanner, pp.1-33
- Marshall Space Flight Center. National Aeronautics and Space Administration.
 Preferred Reliability Practices: Selection of Electric Motors for Aerospace
 Applications. Practice No. PD-ED-1229. Huntsville: NASA, 2010. Print. 1999
- Markovic, Marko & Hodder, André & Perriard, Yves. (2009). An analytical determination of the torque-speed and efficiency-speed characteristics of a BLDC motor. 10.1109/ECCE.2009.5316437.
- 8. Zupp, George A. "An Analysis and a Historical Review of the Apollo Program
 Lunar Module Touchdown Dynamics." Lunar and Planetary Institute, National

- Aeronautics and Space Administration, Jan. 2013, https://www.lpi.usra.edu/lunar/documents/.
- Rozas, Patrick, and Allen R. Cunningham. Lunar Module Landing Radar and Rendezvous Radar. National Aeronautics and Space Administration, 1972.
- 10. Zhou, Yuan & Lu, Yafei & Hei, Mo & Liu, Guangcan & Fan, Dapeng. (2013).
 Motion control of the wedge prisms in Risley-prism-based beam steering system
 for precise target tracking. Applied optics. 52. 2849-57. 10.1364/AO.52.002849.
- 11. Cham, Chin-Long & Samad, Zahurin. (2014). Brushless DC Motor Electromagnetic Torque Estimation with Single-Phase Current Sensing. Journal of Electrical Engineering and Technology. 9. 10.5370/JEET.2014.9.3.866.
- 12. Li, Anhu & Sun, Wansong & Yi, Wanli & Zuo, Qiyou. (2016). Investigation of beam steering performances in rotation Risley-prism scanner. Optics Express. 24. 12840. 10.1364/OE.24.012840.